

# **An EMG-based Method for Finger Gesture Recognition**

Master Thesis

**Ioannis Agalliadis**

This work was submitted to the  
**Department of Medical Informatics**  
**RWTH Aachen University, Germany**

Adviser(s):

Dr. Stephan Jonas  
Marko Jovanović

Examiners:

Univ.-Prof. Dr.med. Dr.rer.nat. Dipl.-Math. Klaus Kabino  
Prof. Dr. Jan Borchers

Registration date: 2017-12-13  
Submission date: 2017-04-10



## Eidesstattliche Versicherung

Agalliadis, Ioannis

Name, Vorname

359894

Matrikelnummer (freiwillige Angabe)

Ich versichere hiermit an Eides Statt, dass ich die vorliegende ~~Arbeit/Bachelorarbeit~~/Masterarbeit\* mit dem Titel

An EMG-based Method for Finger Gesture Recognition

selbständig und ohne unzulässige fremde Hilfe erbracht habe. Ich habe keine anderen als die angegebenen Quellen und Hilfsmittel benutzt. Für den Fall, dass die Arbeit zusätzlich auf einem Datenträger eingereicht wird, erkläre ich, dass die schriftliche und die elektronische Form vollständig übereinstimmen. Die Arbeit hat in gleicher oder ähnlicher Form noch keiner Prüfungsbehörde vorgelegen.

Aachen, 10.04.2018

Ort, Datum

Unterschrift

\*Nichtzutreffendes bitte streichen

### Belehrung:

#### § 156 StGB: Falsche Versicherung an Eides Statt

Wer vor einer zur Abnahme einer Versicherung an Eides Statt zuständigen Behörde eine solche Versicherung falsch abgibt oder unter Berufung auf eine solche Versicherung falsch aussagt, wird mit Freiheitsstrafe bis zu drei Jahren oder mit Geldstrafe bestraft.

#### § 161 StGB: Fahrlässiger Falscheid; fahrlässige falsche Versicherung an Eides Statt

(1) Wenn eine der in den §§ 154 bis 156 bezeichneten Handlungen aus Fahrlässigkeit begangen worden ist, so tritt Freiheitsstrafe bis zu einem Jahr oder Geldstrafe ein.

(2) Straflosigkeit tritt ein, wenn der Täter die falsche Angabe rechtzeitig berichtigt. Die Vorschriften des § 158 Abs. 2 und 3 gelten entsprechend.

Die vorstehende Belehrung habe ich zur Kenntnis genommen:

Aachen, 10.04.2018

Ort, Datum

Unterschrift



## Abstract

---

Wearable devices have been evolving over the last years. The integration of sensors on them encourages scientists to use wearable devices more frequently as they are cheaper and the purchasing accessibility is easier than other specialized devices. In this work, we will use a gesture control armband called Myo. Myo is equipped with a gyroscope, magnetometer, accelerometer and a set of electromyographic (EMG) sensors. Along with the Myo we will use a cell phone which receives the signals from the Myo. The focus point of this master thesis is to research different features based only on EMG signals coming from finger movements. EMG is a signal measurement of the electrical activity of the muscles and is one of the most common sources of information used to study muscle function and neurological disorders. One of the main reasons behind that is that we want to correctly detect finger movements using only the EMG signals that are associated only with arm muscles responsible for motoring the fingers. Also, the existing literature is limited on finger gesture recognition using non-intruding device such as Myo [1]. The goal of this master thesis is to apply the earned knowledge to Myo controlled prosthetic arms worn by amputees that have lost some or all of their fingers or patients that have deficiency of moving their fingers due to a stroke, tendinitis, or peripheral neuropathy. The fact that each finger has a different degree of freedom (DoF) gives us the chance to detect various finger gestures. The most trite ones which we will examine are the extension and the flexion of a finger or a group of fingers. In particular, the thumb can be flexed and extended (2 DoF). The rest of the fingers can be flexed and extended in one direction (1 DoF). The need of a solid classification between these two different kind of movements is imperative. What's more, there can be more combinations such as holding three fingers (thumb excluded) as a cluster and moving forward backward the remaining free finger. The increasing degree of complexity of the different finger gestures plays a significant role in order to have a more complete detection cover over the whole spectrum of finger gestures. After the collection of the recordings, we will introduce a preprocessing stage which will help us in extracting features from the raw data. In this work, we will use a range of methods such as root mean square (RMS), moving average (smooth), Short-Time Fourier Transform (STFT) and a variety of discrete wavelet transforms. The collection of all feature extraction vectors will then be passed into classifiers and classification errors from each feature will be compared with each other in order to determine the best performance. In the implemented framework we will examine the approach of an Artificial Neural Network (ANN) classifier.



# Acknowledgments

I want to thank my advisers Marko Jovanović and Dr. Stephan Jonas for their scientific assistance and continuous support over this period. Special thanks to Dr. Ekaterina Kutafina for providing me also ideas for my master thesis. I would like to thank also the mHealth group generally for creating a friendly and supportive environment.

Furthermore, I want to thank my family for motivating me to finish my master thesis.

Finally, I want to thank Univ.-Prof. Dr.med. Dr.rer.nat. Dipl-Math Klaus Kabino and Prof. Jan Borchers for the possibility to write this thesis as well as supervising it.



# Contents

<b>1</b>	<b>Introduction</b>	<b>1</b>
1.1	Motivation . . . . .	1
1.2	State of the art . . . . .	3
1.3	Electromyography . . . . .	4
1.4	Stationary signals . . . . .	5
1.5	Non-stationary signals . . . . .	7
1.5.1	Cause of non-stationarity in EMG signals . . . . .	8
1.6	Thalmic Myo . . . . .	8
1.7	IMU of the Myo Armband . . . . .	9
1.8	Gesture Recognition . . . . .	10
1.9	Armband positioning . . . . .	10
<b>2</b>	<b>Methods</b>	<b>13</b>
2.1	Pipeline summary . . . . .	13
2.2	Data collection . . . . .	13
2.3	Cross-Validation . . . . .	14
2.4	Windowing . . . . .	16
2.4.1	Windowing in current work . . . . .	16
2.5	Feature extraction . . . . .	17
2.5.1	Moving average . . . . .	17
2.5.2	Root mean square . . . . .	18
2.5.3	Short-time Fourier transform . . . . .	18
2.5.4	Wavelet Analysis . . . . .	22
2.5.5	Continuous wavelet transform . . . . .	22
2.5.6	Discrete wavelet transform . . . . .	23
2.5.6.1	Haar wavelet: An example of wavelet function . . . . .	25

2.5.7	Feature extraction in current work . . . . .	26
2.6	Training and classification . . . . .	27
2.6.1	Forward selection, backward elimination . . . . .	27
2.7	Artificial intelligence . . . . .	28
2.7.1	Biological and artificial neural networks . . . . .	28
2.7.2	Artificial neural networks . . . . .	30
2.7.3	Deep learning . . . . .	31
2.7.4	Deep learning architecture . . . . .	32
2.7.5	Deep feed forward networks . . . . .	32
2.7.6	Learning Conditional Statistics . . . . .	34
2.7.7	Common Activation Functions . . . . .	35
2.7.8	Identity Activation Function . . . . .	36
2.7.9	Logistic Sigmoid . . . . .	36
2.7.10	Hyperbolic Tangent . . . . .	36
2.7.11	Rectified Linear Units . . . . .	37
2.7.12	Softmax function . . . . .	38
2.7.13	Minimization of the cost function . . . . .	38
2.7.14	Backpropagation . . . . .	41
2.7.15	Summary of training neural network . . . . .	42
2.8	Data evaluation . . . . .	43
<b>3</b>	<b>Results</b>	<b>47</b>
3.1	Parameter adjustment . . . . .	47
3.2	Final evaluation . . . . .	49
<b>4</b>	<b>Discussion</b>	<b>55</b>
4.1	Parameter Adjustment . . . . .	55
4.1.1	Increase on the window step . . . . .	55
4.1.2	Forward Selection, Backward Elimination: a hybrid approach .	56
4.2	Evaluation results . . . . .	56
<b>5</b>	<b>Conclusion</b>	<b>59</b>
5.1	Future Work . . . . .	60
5.1.1	Size of data . . . . .	60
5.1.2	Amount of features and reduction of the feature vector . . . . .	60
5.1.3	Network Architectures . . . . .	61

<b>Bibliography</b>	<b>63</b>
<b>List of Figures</b>	<b>68</b>
<b>List of Tables</b>	<b>71</b>
<b>A Appendix</b>	<b>73</b>
A.1 List of Abbreviations . . . . .	73



# 1

## Introduction

### 1.1 Motivation

It is estimated that there are nearly two million people living with limb loss in the United States [2]. Among those living with limb loss, the main causes are vascular disease (54%) including diabetes and peripheral arterial disease trauma (45%) and cancer (less than 2%) [2]. Approximately 185,000 amputations occur in the United States each year [3]. In 2009, hospital costs associated with amputation totaled more than \$8,3 billion [4]. In the work of Robbins et al. they estimated that nearly half of the individuals who have an amputation will die within 5 years due to vascular disease. This is higher than the five-year mortality rates for breast cancer, colon cancer and prostate cancer [5]. Partial hand amputation with loss of one or more fingers, is the most prevalent upper limb amputation [6]. Since hand and finger dexterity requires muscle in the forearm and since ~70% of all upper limb amputations are distal to the elbow this makes the case for the development of hand prostheses with a high degree of dexterity [7, 8]. From the above mentioned we can conclude that the need for the development of prosthetics that can successfully translate the electrical signals from the nerves into the correct finger gesture motion is of great importance. In this work, we will propose a pipeline in order to show how to prepare these raw signals into meaningful input for the powerful artificial neural networks. Fingers are the most used limbs of the human body which help in sensing and manipulating objects. Moreover, finger motions enable humans to express our feelings. One can understand that the variety of finger gestures are endless as they are used from controlling physical objects to expressing intangible ideas. The possibility of employing algorithms to recognize this whole spectrum of finger motions can give an extensive insight into human's everyday life. The mobile devices are some of the physical objects that humans are carrying on them everyday while walking, running, or just waiting for the bus to come. By moving our fingers, we are able to control the user interface of these mobile devices by selecting, adding and deleting elements. Therefore, finger gesture recognition is also significant for human-computer interaction.

There are different kind of mobile devices such as smart watches, mixed-reality-glasses, mobile phones and tablets. Smart watches and glasses due to their small surface promote the idea of an immersive usage with micro-interactions as the usage of onscreen keyboards seems to be impossible. On the contrary, mobile phones and tablets due to their bigger screen have already replaced a great percent of computers. The increasing interest of consumers to control more with smaller, mobile devices gives the chance to wearable technology to emerge. Most of the wearables nowadays do not have keyboard or a wide screen so it is necessary to employ gesture recognition technology. Thus, the need for hands-free human-machine interfaces will help many disabled people who have difficulty to access assistive robotic systems and rehabilitation devices.

At present, there are various methods for capturing and recognizing finger gestures, such as video signal, image analysis, electromyography (EMG) [9, 10, 11, 12]. Many researchers tried to capture finger gestures with cameras but the poor lighting conditions leads to misclassifications. Moreover, the usage of sensing gloves as well as the utilization of capture motion techniques burden the labs with expensive equipment and cost of expertise personnel. Furthermore, most of the existing EMG gesture recognition techniques involve special sensors made for a certain lab that are not available in the science community and therefore experiments cannot be repeated accurately. In this work, the use of EMG signals acquired by the hand of the subjects will be used to detect finger gestures. Myo is a gesture control armband which can acquire among other data, EMG signals.

In the last decade, great progress was made in the area of gesture controlled devices. Nod [13], Mycestro [14] and Myo [1] are some of the devices that made the major breakthrough in this industry. The aforementioned devices are successfully controlled with the user's hand gestures thanks to the integrated sensors such as gyroscope, magnetometer, accelerometer and EMG sensors. Scientists soon came to realise that these devices can help not only in controlling basic remote control functionalities such as changing the volume and the brightness of the sound and video respectively, control basic video flow functionalities such as play, pause, rewind and forward and navigate through different channels but also assist them in gathering data that will help them develop their own ideas and concepts on various fields. These techniques can be useful in designing human machine interfaces, control prosthetics and robots and help in rehabilitation for people with motor disorders. Myo is one of these wearable devices that opened new fields in research.

The aim of this work is to find the most accurate classifications between the different finger gestures. Firstly, we acquire the EMG signals and the video with the recorded finger movement from the cell phone. Then, we eliminate all possible artifacts which happen due to the variable frame rate of the cell phone's camera. After the elimination of the artifacts, we segment the total EMG signal to smaller parts which represent the candidate movements which will be classified, for example flexion and extension of the thumb. Then, the segmented data are separated into five folds for the training data with which we will train the classifiers and five folds for the testing data with which we will test the newly trained network and one evaluation fold. After the separation of the data, we will pre-process the raw data with root-mean-square (RMS), moving average (smooth), short-time fourier transform (STFT) and different discrete wavelet transforms (DWT). With the processed data, the classifiers are trained with each training fold and then tested with the corresponding test fold and the accuracies are calculated. The final outputs are tested with the evaluation

fold. The most accurate features will help us to determine which training folds we will conjuct to re-train the network with them.

To sum up, the current work will add knowledge on how EMG signals coming from finger motion should be preprocessed and classified in order to get accurate classifications. This will give an insight on how the preprocessing of EMG signals can improve the accuracy and efficiency of muscle-controlled devices. This will enable people with motor disorders to better control exo-skeletons such as artificial fingers or arms in cooperation with wearable devices such as the Myo. Myo has the dynamic of an out-of-the box product which can be used as a potentially lower-cost alternative to other mind-controlled devices.

## 1.2 State of the art

Nymoen et al. developed a musical instrument prototype aimed to investigate the use of Myo armband with various instrumental actions [15]. Researchers at the Johns Hopkins University Applied Physics Laboratory have already developed a new surgical technique that allows an amputee to control a modular prosthetic limb with two Myo armbands [16]. Kutafina et al. proposed to use the Myo wearable armband to measure correctness of hand washing for mobile learning which is an important part of medical education [17]. Yang developed a method to tele-control a robot arm to imitate human writing skills using electromyography (EMG) signals which were acquired by the Myo armband [18]. Dash et al. created a novel algorithm which converts the hand movements in the air into a sequence of 2D coordinates on a 2D plane[19]. Their approach provides a recognition module to predict the content of the document created in air. Their algorithm employs deep learning methods which uses the sensor data and the visualizations created by their algorithm. Kosmidou and Hadjileontiadis analyzed EMG and IMU data with intrinsic-mode entropy to recognize Greek Sign Language (GSL) isolated signs[20]. Cheng and Liu adopted a discrete wavelet transform (DWT) to analyze the acquired surface EMG signals to recognize successfully different emotions [21]. Ververidis et al. are researching features such as muscle total pressure, flexors pressure, tensors pressure and gesture stiffness for the purpose of identifying differences in performing the same gesture across different pottery constructions [22].

In all of the above work, the wrist motion of the hand such as the radial and ulnar deviation, wrist pronation/supination and wrist flexion/extension are extensively researched whereas the discrimination of the intention and the control of the fingers motion by surface EMG signals from a human arm still remains ambiguous. In this work, we will try to deepen our knowledge on detection of finger gestures, acquired from the arm of the subject with the EMG sensors of Myo armband. The uniqueness of this work is that the results of this work will be based only on EMG signals coming from the muscles of the forearm, acquired by the Myo device, leaving Inertia Measurement Unit (IMU) data out of the equation. Focusing only on the motion of the fingers, there is no need to set the arm of our subject in motion, therefore we keep it still in a fixed position. Furthermore, the mobility of the Myo as it is wireless and connects to a PC or a mobile phone via Bluetooth connection can only be added to the advantages. Last but not least, Myo armband is the most economic solution

for surface electromyography as it costs 170 euros while the cheapest portable electromyograph system costs around 4500 euros [23].

## 1.3 Electromyography

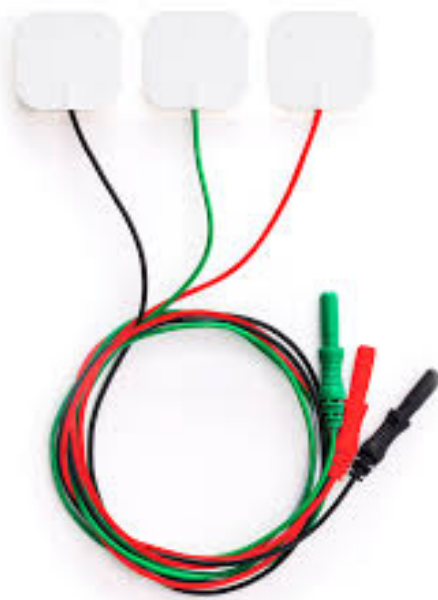
Electromyography is a method for recording the electrical activity produced by muscles. The electrical nerve impulses are transmitted from the brain to the muscles of the arm, which in this work we are studying, via the nervous system. To measure and quantify the electrical nerve impulses EMG has transceivers that help to transmit or receive these electrical impulses. Depending on where the sensor is placed we can conclude which muscles are contracted and how strong the contraction is.

There are two kinds of EMG sensors: the intramuscular Fig 1.1 and the surface EMG recording electrodes Fig 1.2 . With intramuscular electrodes we can track which



**Figure 1.1** Disposable Hypodermic Needle Electrodes[24]

exact muscle is contracting and can get a precise signal resolution from each muscle. The disadvantage is that the procedure is invasive which can become unpleasant for the patient. On the contrary, surface electrodes are placed on the patient's skin, in our case Myo's electrodes, to measure the electrical impulses and are non-invasive which means that they do not provoke any physical discomfort to the patient. The disadvantage is that they are restricted to superficial muscles which induces that it cannot track the electrical activity of one muscle but captures all signals from the muscles in the vicinity of the sensor. This phenomenon is also known as cross-talk [26]. In the forearm there are many different muscles each in different distance from the surface electrode. If an adjacent muscle is active rather than the one directly below the electrode, a crosstalk signal can be detected and misinterpreted as originating from the muscle of interest. The resulting signal is an estimate of the overall muscular activity from the adjacent muscles. Another restriction of the surface electrodes, is that the final output signal is also influenced by the patient's traits such as



---

**Figure 1.2** EMG Surface Electrodes[25]

---

percent of skin fat, hairiness and perspiration. Fatty skin tissue lead to distortion of the signal and hairiness hinders the contact between the sensor and the patient's skin.

## 1.4 Stationary signals

Before analyzing the reason EMG signals are non-stationary signals we will explain what a stationary and a non-stationary signal is. A signal is stationary if its frequency is not changing with respect to time. When we generate a sine wave we determine the frequency and keep it constant. Ergo, the frequency of the sine wave is constant through time and hence this signal is an example of a stationary signal. Stationarity is linked with the behavior of the frequency and has nothing to do with the time varying amplitude of the wave [27]. In Fig. 1.3 we see a stationary signal which in this case is a sine wave. We observe that its frequency is constant whereas the amplitude varies. In the following figure we plot the equation  $y = \sin(2\pi 10t)$ .

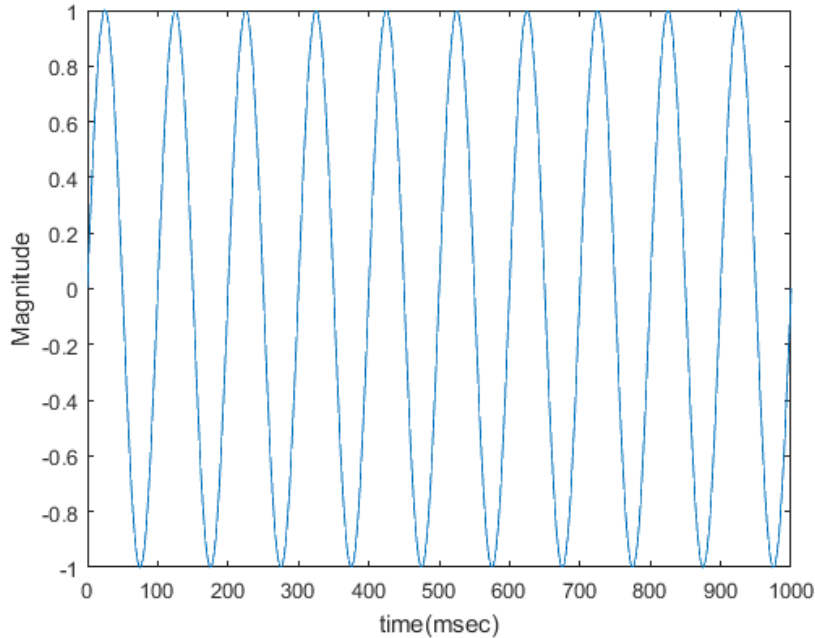


**Figure 1.3** Sine wave of 10 Hz sampled using a sampling frequency of 1000 Hz.

A signal can be also stationary when even it has different frequencies, they do not change over time. If the frequencies of a multitone sine wave do not change over time, regardless of how many frequency components the wave is consisted of, then the signal is stationary. A multitone wave can be written as the Equation 1.1:

$$y = A_1 \sin(\omega_1 t + \phi_1) + A_2 \sin(\omega_2 t + \phi_2) + A_3 \sin(\omega_3 t + \phi_3) \quad (1.1)$$

Next, is the waveform of a multitone signal:

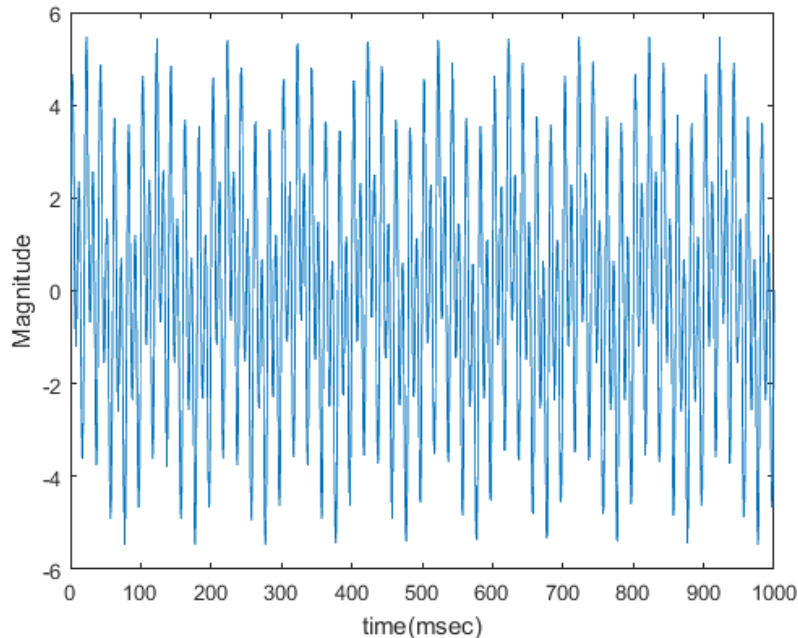


**Figure 1.4** Multitone sine wave of 10, 50 and 100 Hz sampled using a sampling frequency of 1000 Hz.

Although, its waveform is more complicated than the previous one, it is a stationary signal as its frequencies remain constant through time.

## 1.5 Non-stationary signals

Let's assume a multitone signal whose duration is divided into four intervals. Let's assume frequency  $f_1$  is present in the first interval,  $f_1$  and  $f_2$  in the second interval,  $f_1$ ,  $f_2$  and  $f_3$  present in the third interval and  $f_1$  in the fourth interval. We observe that the frequencies are changing from interval to interval. Thus, this wave qualifies as non-stationary. For example in Fig. 1.5 we consider a non-stationary wave with frequency 10 Hz for the first interval, 10 and 50 Hz for the second interval, 10, 50 and 100 Hz for the third interval and 10 Hz for the fourth interval. In Equation.

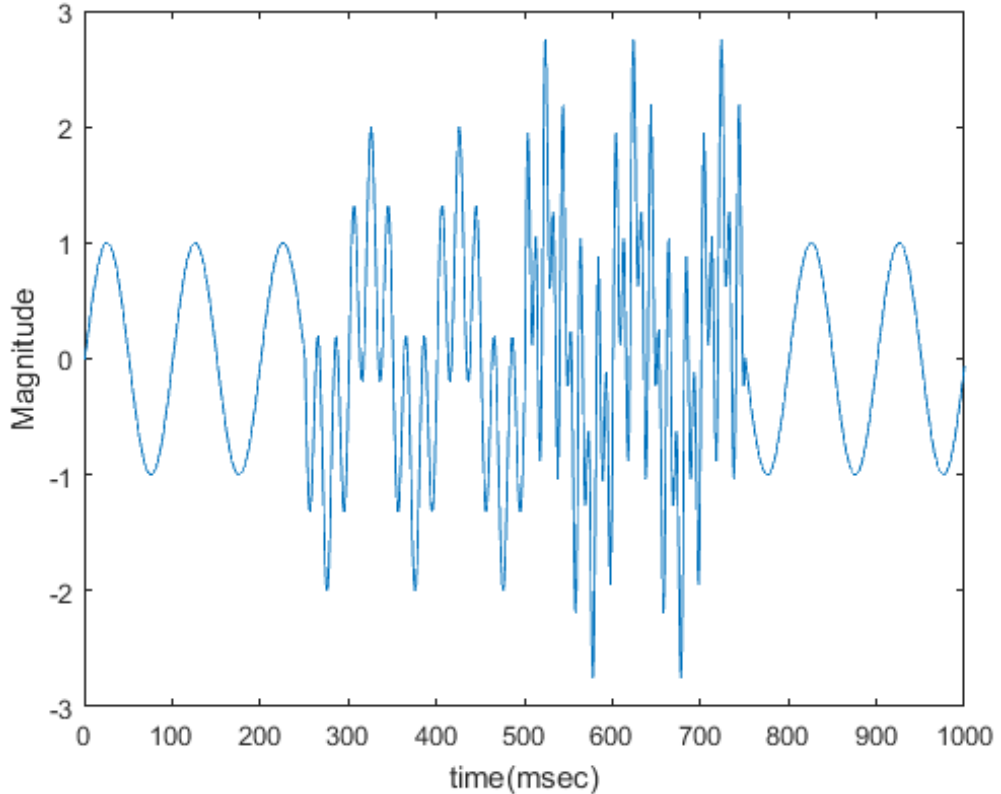


**Figure 1.5** Non-stationary multitone sine wave of 10, 50 and 100 Hz sampled using a sampling frequency of 1000 Hz.

1.2 we give the mathematical formulation for such a signal.

$$x(t) = \begin{cases} A_1 \sin(\omega_1 t + \phi_1) & 0 \leq t \leq t_1 \\ A_1 \sin(\omega_1 t + \phi_1) + A_2 \sin(\omega_2 t + \phi_2) & t_1 \leq t \leq t_2 \\ A_1 \sin(\omega_1 t + \phi_1) + A_2 \sin(\omega_2 t + \phi_2) + A_3 \sin(\omega_3 t + \phi_3) & t_2 \leq t \leq t_3 \\ A_1 \sin(\omega_1 t + \phi_1) & t_3 \leq t \leq t_4 \end{cases} \quad (1.2)$$

### 1.5.1 Cause of non-stationarity in EMG signals

During muscle contractions, joint angles various muscles work together in order to perform a certain movement. This may involve the recruitment or the de-recruitment of muscles for rapid contributions, which will introduce non-stationarities to the final EMG signal. Also, due to changes in the joint angles, the underlying muscles change position relative to the recording electrodes. This results in the electrodes not to be correctly positioned above the muscles and this affects sequentially the recorded frequency. Last but not least the variability of the length of the muscle fibers can influence as a scaling factor to the power spectrum of the EMG signal [28]. Furthermore, when the muscle is getting tired, metabolites are accumulated over time in the muscle. The metabolites result in a decrease of conduction velocity of the motor action along the muscle fibers. This affects the power spectrum of EMG signals and thus introduces non-stationarities in the EMG signal [28].

## 1.6 Thalmic Myo

Thalmic Myo shown in Fig. 1.6 was developed by Thalmic Labs in 2014 [29]. It is worn on the forearm and enables the user not only to control a computer as a computer mouse would do but also can provide the control of various gadgets such as quadcopters and gyroballs with the help of hand detection.

Large parts of the Myo's software [30] is publicly available and Thalmic labs provides access to development kits for most of the operating systems. Furthermore, they explain their ideas behind the implementation and help the developers to extend their product by adding more functionalities to it.

The Myo is extendable from 19 cm to 43 cm forearm circumference. The Myo armband is 1.1 cm thick and weights 93 grams.

As Myo is a wearable device, it is programmed to transfer the collected data to another device. Thalmic Myo uses Bluetooth connection as the communication protocol between the Myo and the client. The structure of Myo is equipped with eight stainless EMG sensors designed for recognizing hand gestures and movements. It also consists of a 9-axis (IMU) Inertial Measurement Unit used to detect arm movements. The IMU consists of a 3-axis gyroscope, a 3-axis accelerometer and a 3-axis magnetometer.

The accelerometer and gyroscope are basic common sensors that come with every mobile phone device and smart wearable devices such as fitness trackers. The novel approach of Myo is the embedded EMG sensors.

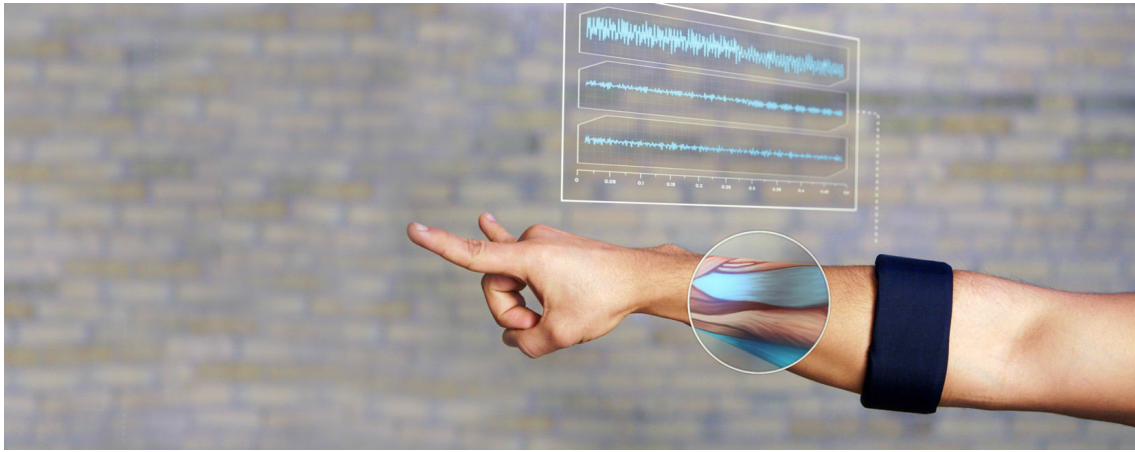


**Figure 1.6** Myo armband

Myo uses five gestures to interact with the environment shown in Fig 1.7, these five gestures include fist, double tap, finger spread, wave left and wave right.



**Figure 1.7** Gestures recognized by Myo

Myo's sampling frequency is 200 Hz that means that it provides 200 EMG samples per second. Therefore, frequencies up to Nyquist frequency of 100 Hz can be detected. When the Bluetooth connection is set up the users are able to map each gesture into a particular input event in order to interact and communicate with the connected devices.

## 1.7 IMU of the Myo Armband

Although we will not use in this work the offered IMU data. The inertial measurement unit consists of multiple single sensors in order to acquire accelerometer, gyroscope and orientation data. The IMU sensors are contained in the fourth pod as in Fig. 1.8, where also the Bluetooth, the Universal Serial Bus (USB) and two LEDs find place. The sampling frequency for the IMU data is determined at 50 Hz [31].

The accelerometers in the Myo armband measures the acceleration of the forearm. With the help of accelerometers and the provided framework of Thalmic Labs, Myo can detect not only the basic movements of the hand but also more complex movements.

The gyroscopes helps to track the change in the orientation while the armband is rotated and translated by the user's arm. The way the gyroscopes works is that it

simulates an artificial horizon and maintains orientation according to that horizon. The gyroscope provides the user with angular velocity data, which is provided in vector format.

Last but not least, the orientation data indicates which way the Myo armband is pointed in terms of roll, pitch and yaw. The orientation data is delivered in two possible formats: angle-velocity and quaternions.




---

**Figure 1.8** EMG channel assignments

---

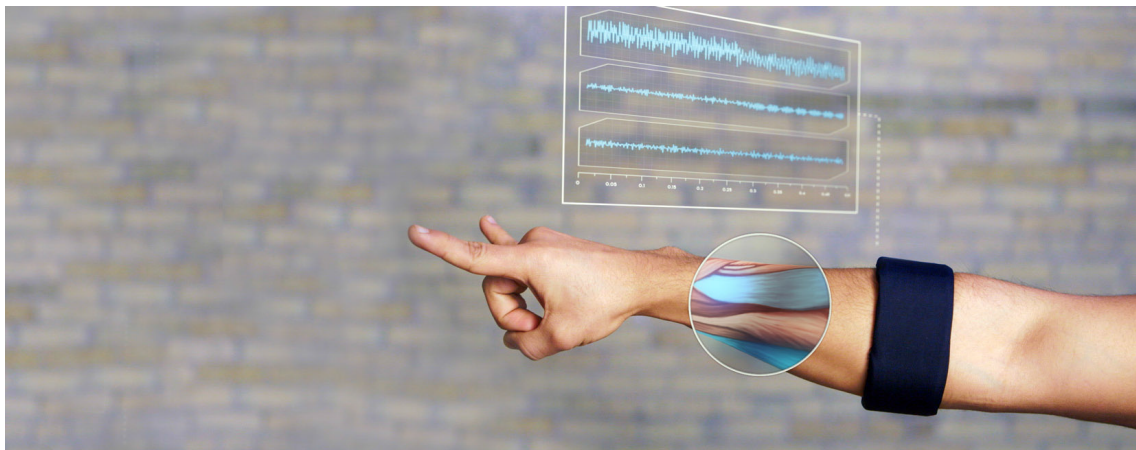
## 1.8 Gesture Recognition

Gesture recognition can be seen as a way for computers to understand body language. The aforementioned supported gestures can help the user to interact with technology but it is restrictive as it limits the total recognized gestures down to five. However, the experienced user can have access to the IMU and EMG data and develop his/her own ideas to recognize custom gestures such as flexion and extension of each individual finger. In this current work, we will use one Myo which we wear in the right arm and fetch EMG signals with it. The arm during all experiments will remain still. Therefore, the IMU data are not needed for this study. The reason for not moving the whole arm, is that we want to study only the individual movements of the fingers with Myo's EMG sensors.

## 1.9 Armband positioning

Myo's position on the user's arm is very important. From that, it depends which sensor is recording which muscle. If we change the position of the sensors during the experiment the values of each of the eight channels will give us different results and we will have not sensible data. Therefore, during the experiment the sensors must be set firmly on the user's arm. Furthermore, during the whole sequence of experiments the Myo must be worn in the same approximately position as best as possible in order to have a homogeneity of results for each channel from each experiment. In the current work, the subject will wear the Myo on top of the right hand after stretching

his/her hand with the back of the hand facing downwards and placing the pod with LED indicator to face towards the wrist.



---

**Figure 1.9** Positioning of Myo in user's forearm. [32]

---



# 2

## Methods

The proposed processing techniques and methods used for evaluating finger movements and recognizing errors requires six steps: (1) removal of artifacts from Electromyography (EMG) data, (2) segmentation of the EMG data into individual movements, (3) division of the EMG data into 11 folds (11 is the number of the features we are preprocessing the EMG data with), (4) windowing, (5) feature extraction, (6) classification. The machine learning model learns the patterns of the preprocessed data by the selected features, segmented individual finger movements. Based on the detection accuracies of each machine learning model, allows us to have feedback on which of the features are working best on the EMG data.

### 2.1 Pipeline summary

In Fig. 2.1 the overview of the system's pipeline is depicted.

### 2.2 Data collection

In Fig. 2.2 we can see how the data are acquired. Firstly, the subject wears the Myo armband in his/her arm and via Bluetooth connection the Myo armband is connected with a mobile phone. After the completion of the corresponding finger gesture the zip folder with the acquired signals and the video recording are uploaded to the cloud. The EMG signals and the video recordings are downloaded to the PC. The video recording is used next, in order to determine the intervals of the gestures we are interested in. Then, we input the frames of interest in the Cutter App, an application implemented by Seiffarth Johannes, and the EMG signals are segmented in the corresponding frame intervals. Also, with the same application

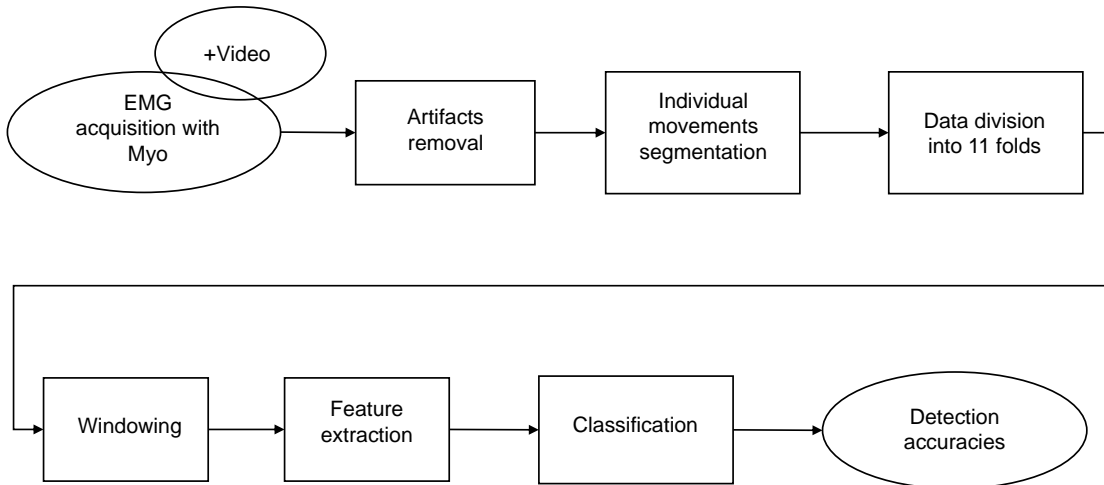


**Figure 2.1** Overview of the pipeline

we can visualize the EMG waveforms of the different recordings and to remove any artifacts. In the current work, due to the variable frame rate of the cell phone's camera the frames of the video did not correspond to the corresponding waveform in time, thus leading to artifacts. This behavior of the mobile device's camera happened unexpectedly during the different takes. Therefore, every recording was examined carefully before segmenting it.

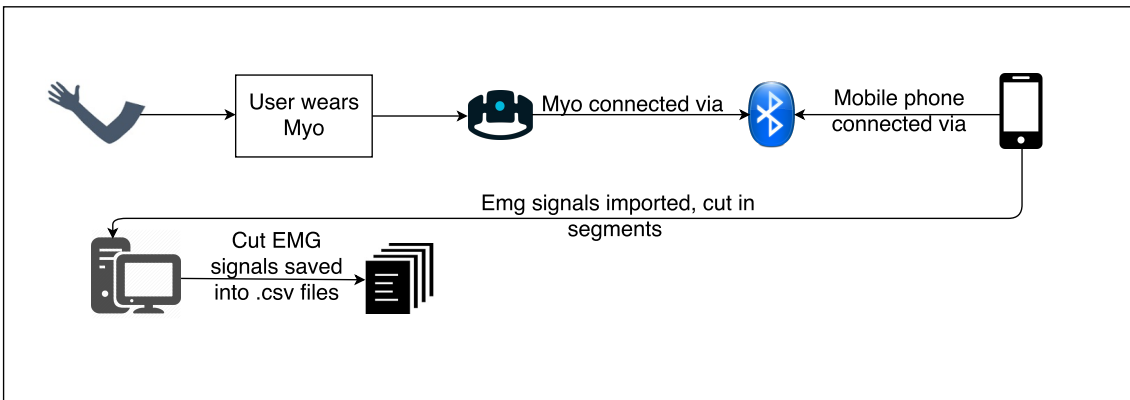


**Figure 2.2** Data collection

## 2.3 Cross-Validation

Next, as the Fig. 2.3 demonstrates, the data are divided into training, testing and evaluation folders. Specifically, we start by removing 20% of the segmented data and we create a evaluation folder with this data. Until the machine learning model is fully developed we do not touch the data from the evaluation folder. In addition, cross validation technique allows to compensate for small data sets and makes our

results more robust. Then, we have to decide on the number of the folds. If we choose a large number of folds we will have too little data in each fold and if we choose a small number of folds, the method will not be serving its purpose. In our case, we choose to create five training and test folds and one evaluation folder. The remaining 80% of the data, will be our train and test data.

After the creation of the evaluation folder, we create the five test folders by dividing randomly the remaining data accordingly to the number of the folders we created. In our case, we take a random 20% from the remaining data and distribute it to each of the five test folders. Then, we create each of the five train folders by combining all the data from the test folders but excluding the folder with the mutual shared number. For example, the train folder with the number one will take all the data from the test folders with the number two, three, four and five thus, excluding the test folder with the number one. This applies for the rest of the train folders. After the completion of all of the above steps, we end up having five folders with train and test data and one evaluation folder storing our segmented EMG signals and ready to input them to our machine learning models.

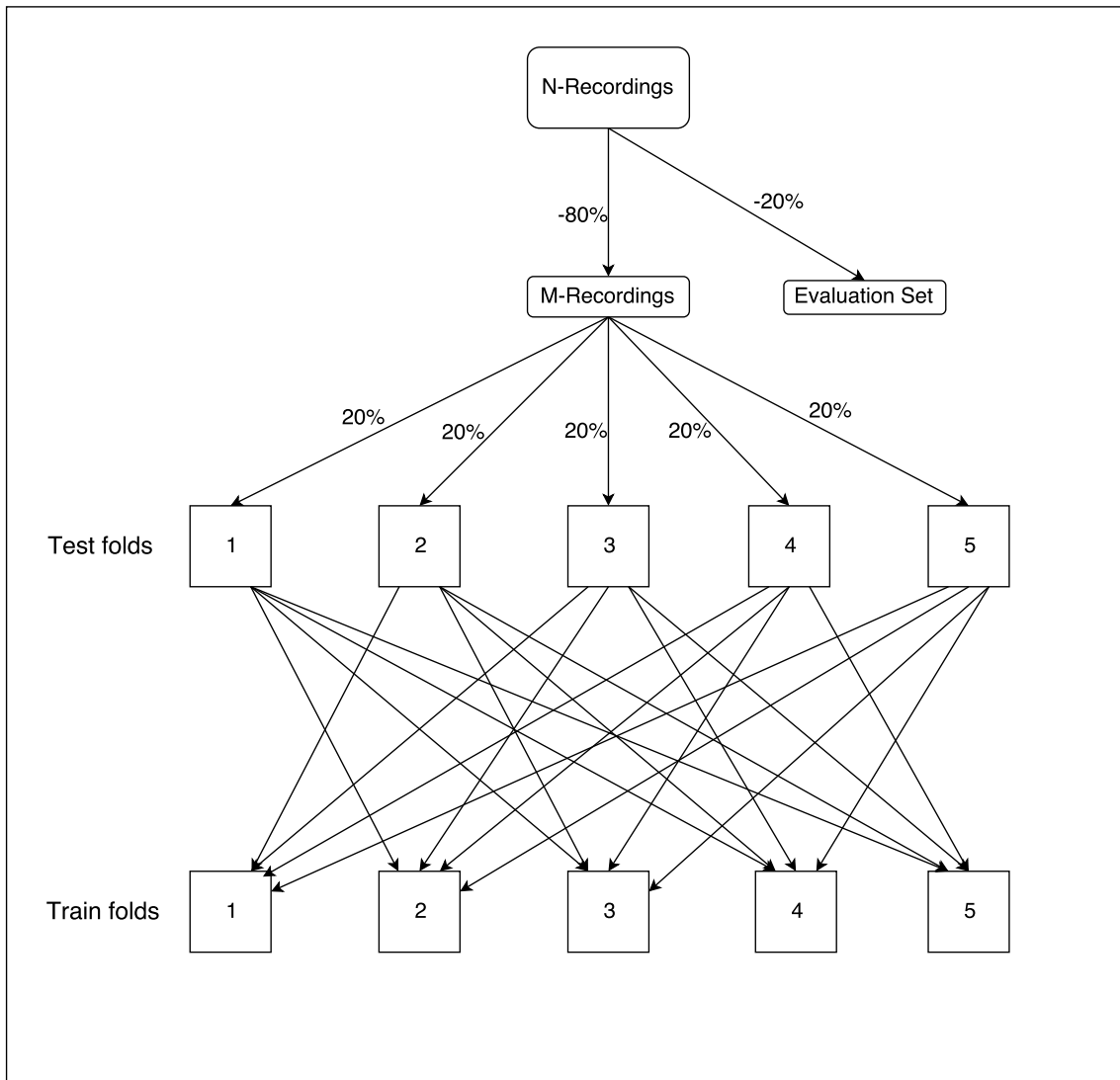


**Figure 2.3** Division of recording into 5 folds

## 2.4 Windowing

Windowing is a common technique in machine learning to improve the detection accuracies. It is a procedure that is applied to the training and testing data before they are fed into the machine learning and thus it can be universally applied, independently of the classification algorithm in use [33].

In order to forward the data into the machine learning algorithm we often have to apply windowing to the data in order to properly format them as an input. In our experiments we acquire raw EMG data from the Myo that are captured at a fixed sampling frequency of 200 Hz. We force the classifier to take a certain perspective on the problem by defining a sample to consist of this set. Windowing is a way to avoid the problem of comparatively long ranges of samples by reducing the input vector's length. We define a window length  $w$  and reshape the input vector in such a way that each input vector contains  $w$  sensor readings. For example, if we acquire the EMG data of one Myo armband and assume a window of size  $w = 10$ , each input vector contains not just 8, but 80 values, corresponding to 10 consecutive readings of the 8 EMG sensors in one Myo armband.

With this technique, each output value corresponds to larger set of sensor readings, more actual muscle activity is mapped to a gesture. This seems to be reasonable approach when looking at the vast differences in resolution: up to 200 sensor readings per second vs. one gesture change every few seconds. In such a manner, this approach forces the classifier to look at the data through a window that shows a more expressive excerpt of the input data.

The disadvantage that comes with windowing is that every value  $w$  that is used creates an artificial connection between those  $w$  values of input data that either may or may not be relevant to determine the corresponding output values. For example, if the window length  $w$  is wide, a window can contain data that belongs to multiple gestures. On the contrary, if the window is narrow it may not contain the necessary number of samples to characterize successfully the multiple gestures. That is why  $w$  needs to be chosen carefully.

A solution to overcome this particular problem of windowing is to create *overlapping* windows. Without overlapping windows each sample is somehow treated with the same weight. However, when someone observes the extracted features from two consecutive frames the change of property between the frames may induce a discontinuity. With the overlapping though, some  $x_i$  of the original input vector will land in multiple windows. With this way, each measurement can be viewed twice but in a different context.

Depending on the value  $o$  which is bounded with  $0 \leq o \leq w - 1$  this can increase the size of the input vector. At the cost of larger vector sizes and effectively more computation time, overlapping windows can reduce the impact of the artificial connection between values that is introduced by windowing.

### 2.4.1 Windowing in current work

In our case, Fig. 2.4 states that we take each train, test and evaluation sets and we apply a window of 128 length with a step of one to each recording. For the sake of computation time we changed the step from one to 64 for the later experiments.

Each row of each recording consists of nine columns where the first column is the timestamp and the rest eight columns are the indicators from the eight EMG sensors. All the produced 128-length windows are concatenated vertically in a final array.

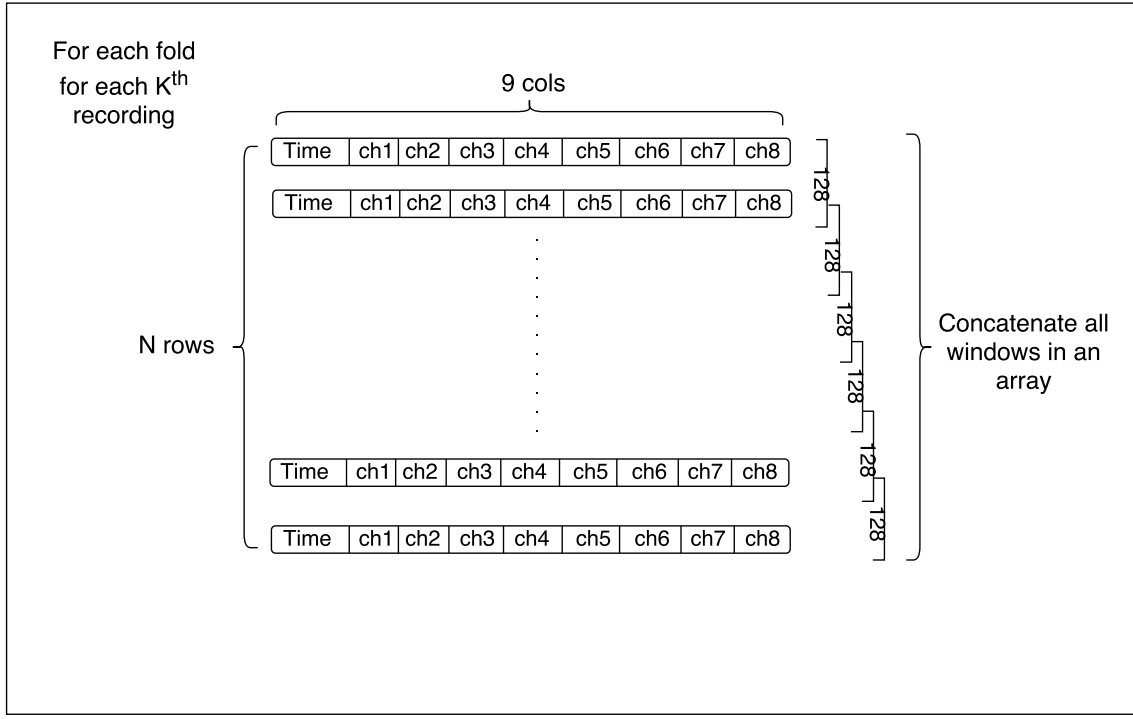


**Figure 2.4** Windowing

## 2.5 Feature extraction

The information extracted from the EMG signals, which are represented in a feature vector, is chosen to help in minimizing the classification error which show us which of the selected features have the possibility for the most efficient identification of the each finger gesture.

In this section we are going to explain further the methods we used to extract the features from the acquired EMG signals.

### 2.5.1 Moving average

The moving average function, calculates a series of averages from successive segments of a series of values. A moving average is used with time series data to smooth out short-term fluctuations as our data are already noisy. The simple moving average is taken from an equal number of data points on either side of a central value. This requires using an odd number of values in the sample window. In our case, moving

average is taken in a window size of five. The definition of the arithmetic mean is given by the following equation [34]:

$$s_i = \frac{1}{n} \sum_{j=1}^{i+n-1} \alpha_j \quad (2.1)$$

### 2.5.2 Root mean square

Root mean square (abbreviated RMS and sometimes called the quadratic mean) is the square root of the arithmetic mean of the squares of a set of values. The equation is following:

$$x_{RMS} = \sqrt{\frac{x_1^2 + x_2^2 + \dots + x_n^2}{n}} = \sqrt{\frac{\sum_{i=1}^n x_i^2}{n}} = \sqrt{\langle x^2 \rangle} \quad (2.2)$$

where  $\langle x^2 \rangle$  is the arithmetic mean of the series  $x_i^2$  [35]. If  $x$  is a row or a column vector,  $x_{RMS}$  is a real-valued scalar.

### 2.5.3 Short-time Fourier transform

STFT is a well known technique in signal processing to analyze non-stationary signals. Particularly, STFT helps to analyze a small section of the signal over time thanks to the *windowing* function applied (e.g., Hann, Gaussian) on the signal. Fig. 2.5 shows us in brief how STFT works. STFT maps a signal into a two-dimensional

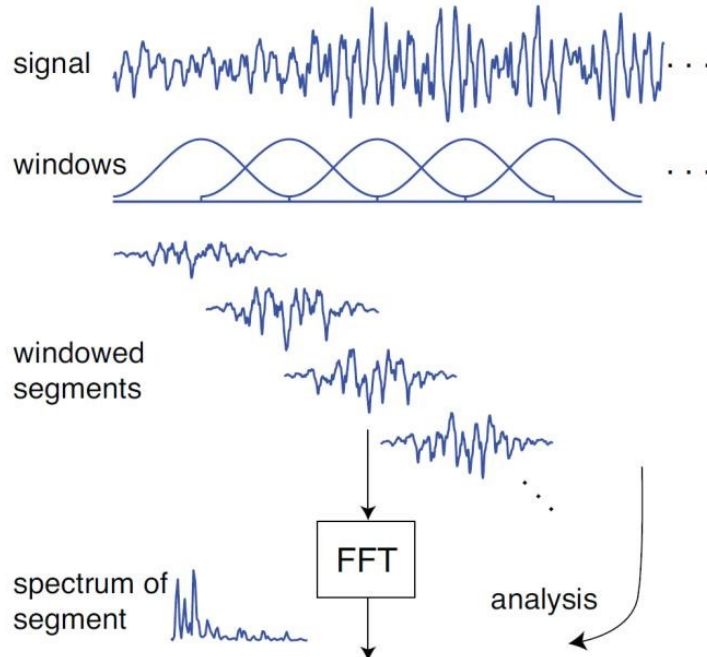


**Figure 2.5** Application of the STFT in the segmented windows [36]

function of time and frequency. Each section, that means  $x[n]w[n - m]$  is Fourier

transformed, and the complex result is added to a matrix, which records magnitude and phase for each point in time and frequency. This can be expressed as:

$$\text{STFT}x[n](m, \omega) \equiv X(m, \omega) = \sum_{n=-\infty}^{\infty} x[n]w[n-m] \exp^{-j\omega n} \quad (2.3)$$

with signal  $x[n]$  and window  $w[n]$ . STFT provides information about when and which frequencies in a signal occurs. One can obtain that information with a limited precision depending on the size of the window. As the size of the time window is the same for all frequencies this constitutes a disadvantage and leads to cutting valuable information. To determine accurately time or frequency one need to vary the window size. The weak point of STFT is that whoever wants to use it will face the problem of resolution. Which means that there is a question of what window size should someone choose. Narrow windows offer good time resolution but poor frequency resolution. Wide windows offer good frequency resolution but poor time resolution [37]. To visualize what we explained with words, in Fig. 2.6 we produce four spectrograms to emphasize between the different effect the window size of STFT has on the signal that is consisted from simple stationary sinusoidal waveforms joined together. The signal is sampled at frequency 400 Hz:

$$x(t) = \begin{cases} \cos(2\pi 10t) & 0s \leq t < 5s \\ \cos(2\pi 25t) & 5s \leq t < 10s \\ \cos(2\pi 50t) & 10s \leq t < 15s \\ \cos(2\pi 100t) & 15s \leq t < 20s \end{cases} \quad (2.4)$$

As we can observe, with the 25 ms window we are able to say with great precision

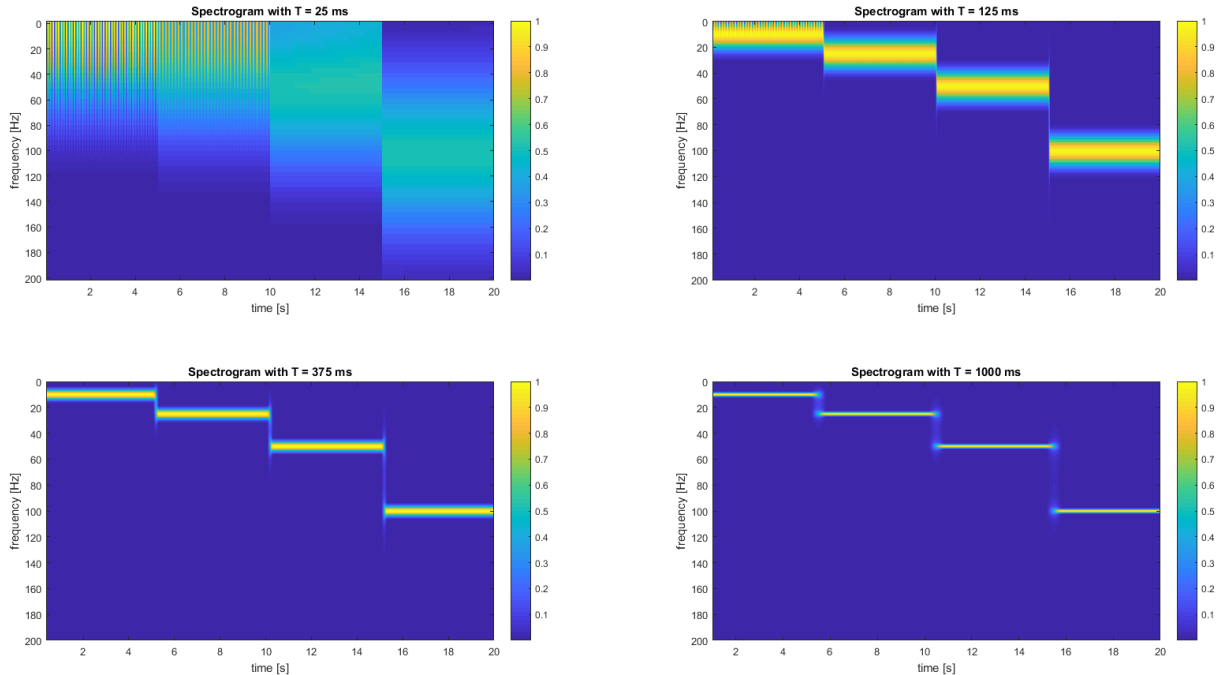


**Figure 2.6** Spectrograms of the thumb extension

when the frequency of the signal changes but to identify which frequencies exist in the signal still remains a difficult task. On the contrary, with bigger window sizes such as with  $T = 1000$  ms we can detect with great precision which frequencies exist in the signal while the determination of the periods when these frequencies happen is difficult to distinguish because of the blur.

The spectrogram we used to visualize the STFT of the signals is generated by the squared magnitude of the STFT. The equation is following:

$$\text{spectrogram}\{x(t)\}(\tau, \omega) \equiv |X(\tau, \omega)|^2 \quad (2.5)$$

In the Fig. 2.7 we can see the spectrogram of a signal coming from the thumb extension and in the Fig. 2.8 we can see the spectrogram of a signal coming from the thumb flexion. The spectrogram can be represented as a visual heat map

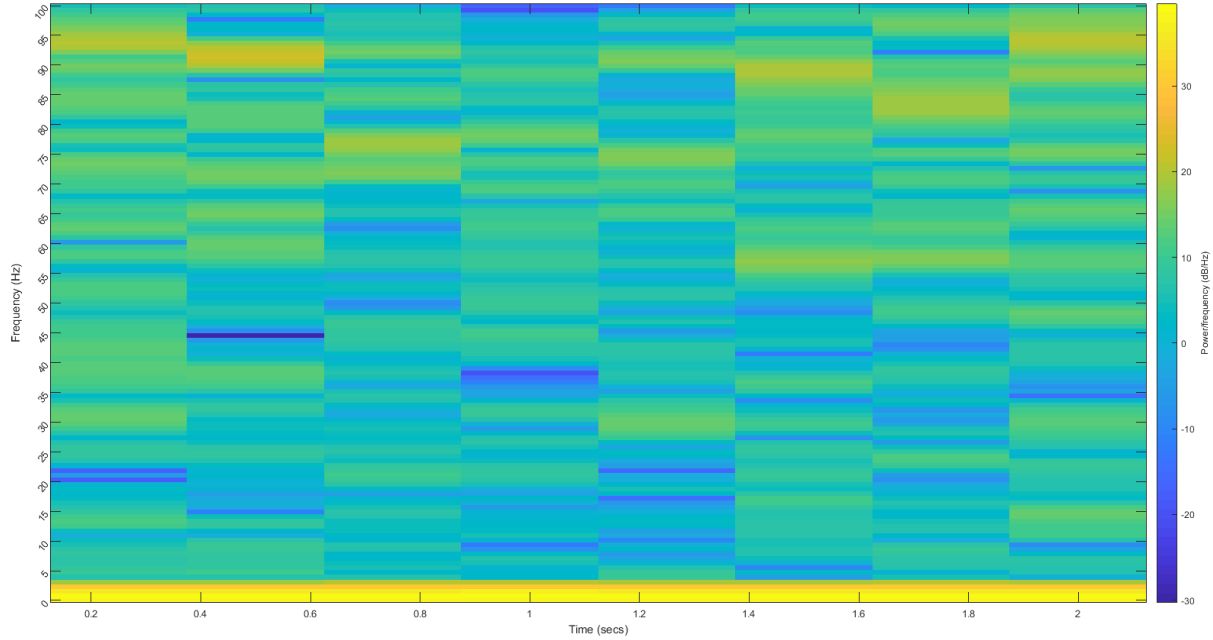


**Figure 2.7** Spectrogram of the thumb extension from Myo's 7th channel

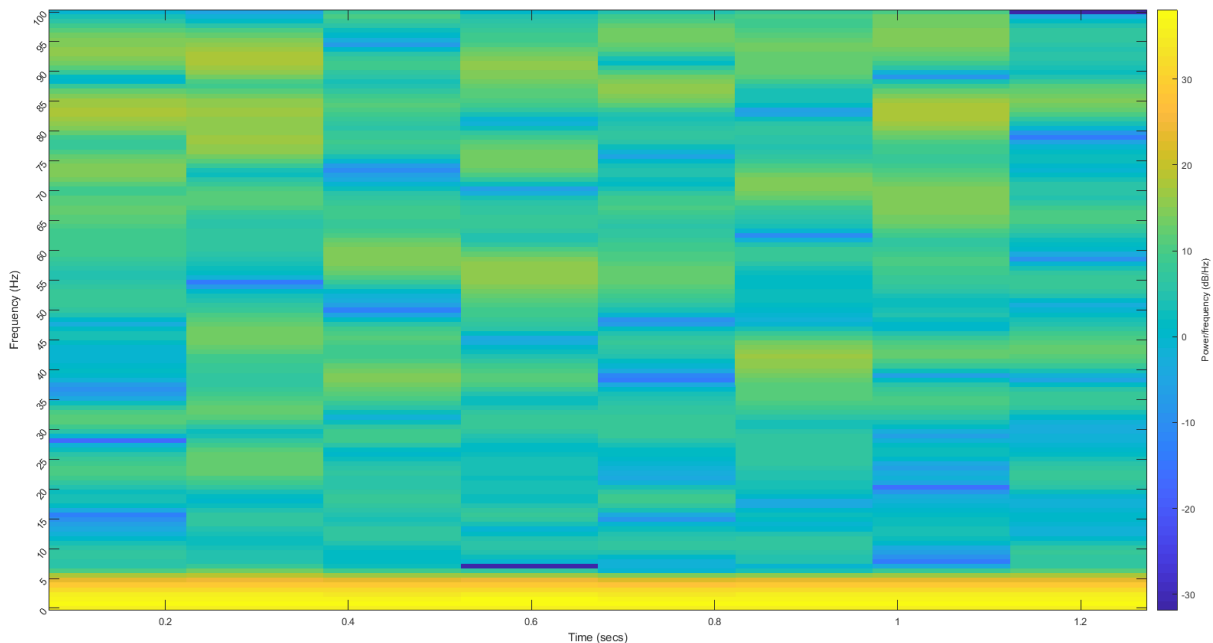


**Figure 2.8** Spectrogram of the thumb flexion from Myo's 7th channel

where the horizontal axis represents the time axis and the vertical axis represents

the frequency axis. In the above image the darker colors visualize for a particular time point and a particular frequency low magnitude. So, the darker the colors the lower the magnitude and similarly the higher in magnitude the frequency component is, the lighter the color.

### 2.5.4 Wavelet Analysis

Wavelet analysis (also called wavelet theory or just wavelets) has attracted much attention in signal processing. In order to overcome the resolution problem with the fixed window size in Fourier Transform a different approach is employed. Like Fourier analysis, wavelet analysis deals with expansion of functions in terms of a set of basis functions. Unlike Fourier analysis, wavelet analysis expands functions not in terms of trigonometric polynomials but in terms of wavelets, which are generated in the form of translations and dilations of a fixed function called the mother wavelet [38].

A wavelet is a little wave oscillation with an amplitude that begins at zero increases and decreases back to zero. The original signal is convoluted with the wavelets. With this way, useful information is extracted from the raw signals.

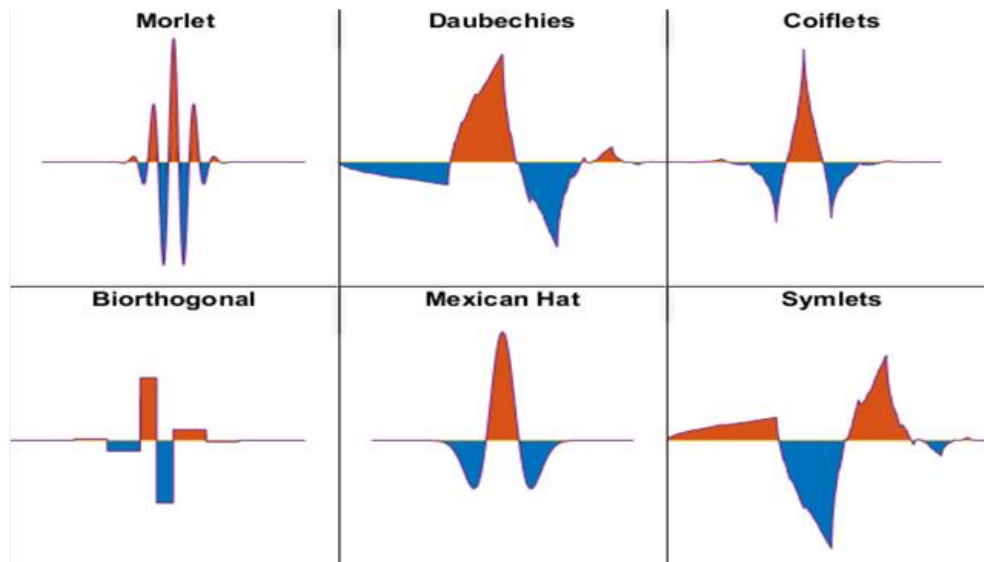


**Figure 2.9** Wavelet families [39]

### 2.5.5 Continuous wavelet transform

The formula for the continuous wavelet transform is:

$$\text{CWT}_\chi^\psi(\tau, s) = \Psi_\chi^\psi(\tau, s) = \frac{1}{\sqrt{|s|}} \int x(t)\psi^*\left(\frac{t-\tau}{s}\right)dt \quad (2.6)$$

where  $\tau$  is translation (location of the window) and  $s$  is scale.  $\psi^*\left(\frac{t-\tau}{s}\right)$  is the **mother wavelet** which we will explain further later.

The most significant difference between STFT and wavelets is that the width of the window is changed in wavelet analysis whereas the window used by STFT is

fixed [40]. For local areas with high frequencies the window size will be shorter whereas for local areas with low frequencies the window size will be longer. The term **mother wavelet** gets its name by two important properties. Firstly, wavelet as it is a small wave (finite length), and mother because all functions with different regions of support stem from a main function, the mother wavelet. This means that mother wavelet acts as a prototype for generating other functions. The translation term is related to the location of the window while it is shifting through the signal. Thus, translation term corresponds to the time information. As we can observe there is no frequency component in the Eq. 2.6. Instead, we have the scale parameter which is  $\frac{1}{frequency}$ . In terms of frequencies, low frequencies (high scales) correspond to a macroscopic information of the entire signal, whereas high frequencies (low scales) correspond to a microscopic detailed information of the signal. High scales (low frequencies) last for the entire duration of the signal while low scales (high frequencies) do not last for the entire duration of the signals but appear from time to time like short bursts.

### 2.5.6 Discrete wavelet transform

The discrete wavelet transform (Discrete Wavelet Transform (DWT)) is an implementation of the wavelet transform using a discrete set of the wavelet scales and translations obeying some rules. DWT is simply a sampled version of Continuous Wavelet Transform (CWT). The Discrete Wavelet Transform (DWT) provides sufficient information for synthesis and analysis of the original signal. DWT is similar to the Fourier transform in that it is a decomposition of a signals in terms of a basis set of functions. In Fourier Transform, the basis set consists of sines and cosines and the expansions has one parameter which is the window length. In wavelet transform, the expansion has two parameters and the wavelets are generated from a single mother wavelet using dilation and offsets corresponding to the two parameters. The formula for the discrete wavelet transform is given by:

$$f(t) = \sum_s \sum_{\tau} c_{s\tau} \psi_{s\tau}(t)$$

where the two-parameter expansion coefficients are given by

$$c_{s\tau} = \int f(t) \psi_{s\tau}(t) dt$$

and the wavelets obey the situation

$$\psi_{s\tau}(t) = 2^{\frac{s}{2}} \Psi(2^s t - \tau)$$

Here  $\Psi$  is the mother wavelet,  $s$  is the scale parameter and  $\tau$  is the translate parameter. DWT applies the same idea as CWT. CWT is a correlation between a wavelet at different scales and the signal with the scale (or frequency) being used as a measure of similarity. By scaling the analysis window, shifting it in time, multiplying it and integrating it over all times, we acquire the CWT of a signal.

In the discrete case, filters of different cutoff frequencies are used to analyze the signal at different scales. The signal is passed through a series of high pass filters

to analyze the high frequencies and it is passed through a series of low pass filters to analyze the low frequencies. The resolution of the signal, which is the amount of detail in the signal, is changed by the different filter operations and the scale is changed by the upsampling and the downsampling (subsampling). Subsampling a signal means that we reduce the sampling rate or removing some samples from the signal whereas upsampling means that we increase the sampling rate by adding new samples to the signal. The procedure starts with passing this signal through a half

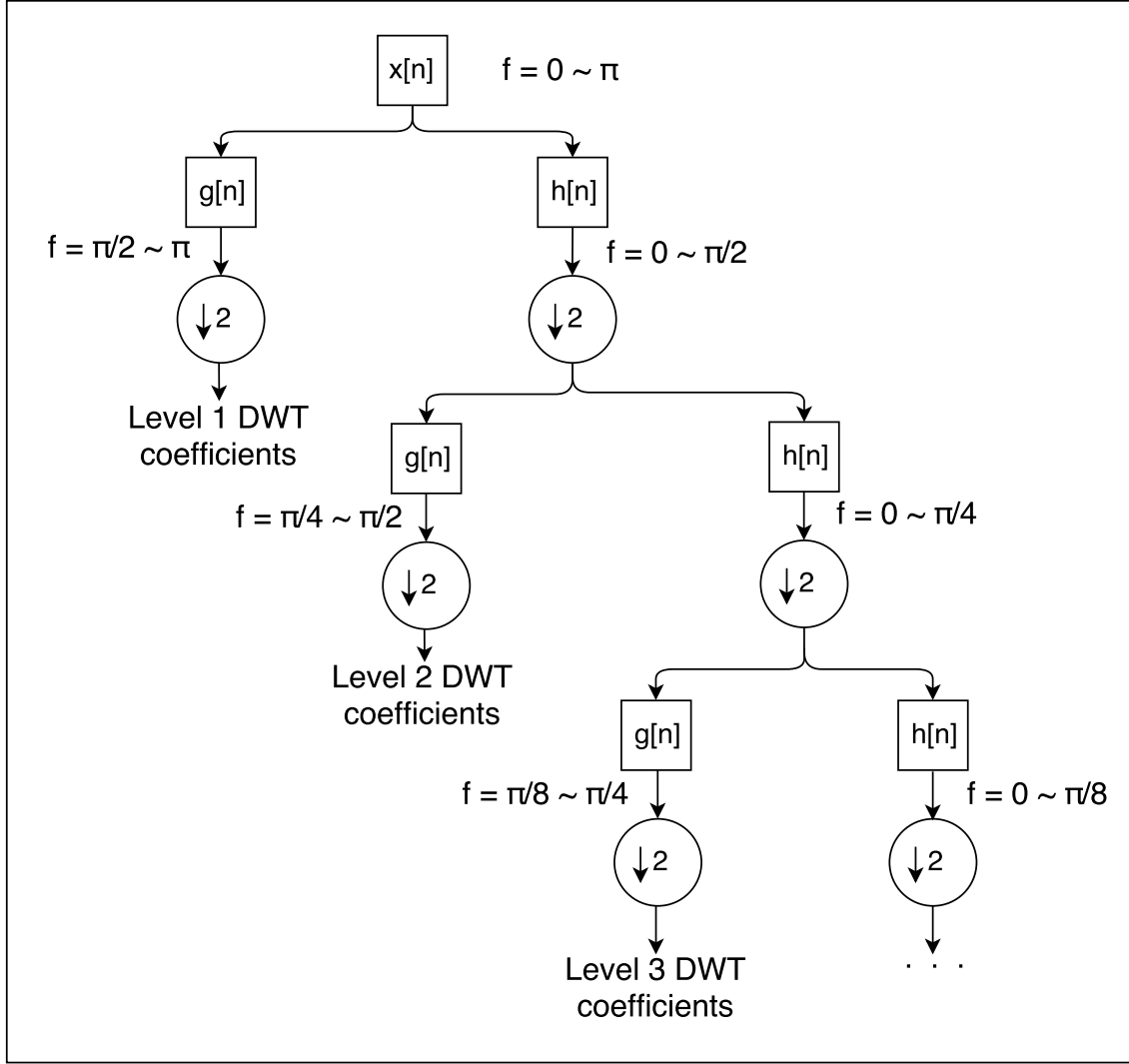


**Figure 2.10** The subband coding algorithm

band digital lowpass filter with impulse response  $h[n]$ . The mathematical operation of convolution corresponds to filtering the signal with the impulse response of the filter. The convolution in discrete time is defined as:

$$x[n] \circledast h[n] = \sum_{k=-\infty}^{\infty} x[k] \cdot h[n-k]$$

The half band lowpass filter removes all frequencies that are above half of the highest frequency in the signal. After passing the half band lowpass filter, half of the samples are eliminated thus leading to a subsampling of the signal by two, causing it to remain with half the number of points. Resolution is related to the amount of

the information in the signal and therefore resolution is halved after the filtering operations. This causes the scale to double. This procedure can be expressed as:

$$y[n] = \sum_{k=-\infty}^{\infty} h[k] \cdot x[2n - k]$$

According to the 2.10 DWT employs two sets of functions, the scaling and the wavelet functions which correspond to low and highpass filters. These filters with the different frequency bands and with different resolutions, decompose the signal into a coarse approximation and detail information [37]. The decomposition is obtained by applying successively highpass and lowpass filtering on the time domain signal. The raw signal  $x[n]$  is passed through a halfband highpass filter  $g[n]$  and a lowpass filter  $h[n]$ . According to the Nyquist's rule, after the filtering, half of the samples are eliminated, since the signal has now a highest frequency of  $p/2$  radians instead of  $p$ . This composes one level of decomposition and can be expressed as:

$$y_{high}[k] = \sum_n x[n]g[2k - n] y_{low}[k] = \sum_n x[n]h[2k - n]$$

where  $y_{high}[k]$  and  $y_{low}[k]$  are the outcomes of the highpass and lowpass filter after subsampling by 2.

Since only half of the number of the samples characterizes the raw signal, the decomposition halves the time resolution whereas the frequency resolution is doubled since the frequency band of the signal spans half the previous frequency band. At every level, the filtering and the subsampling half the number of samples (hence half the time resolution) and half the frequency band spanned (hence double the frequency resolution) [37]. In the Fig. 2.10  $h[n]$   $g[n]$  are lowpass and highpass filters and the bandwidth of the signal at every level is denoted with "f".

The most prominent frequencies in the raw signal will have the biggest amplitude in the DWT. The difference between DWT and the Fourier transform is that the time localization will be preserved. The time localization will have a different resolution depending on the current level we use for the DWT. The length of the signal determines the number of levels that the signal can be decomposed to. For example, if the signal length is 1024, ten levels of decomposition are possible [37].

If the main information is located in the high frequencies, the time localization will be more precise since higher frequencies are characterized by more number of samples. If the main information is located in the low frequencies, the time localization is less precise, since a small number of samples express the raw signal at low frequencies.

### 2.5.6.1 Haar wavelet: An example of wavelet function

The haar wavelet is the simplest kind of wavelet function. The haar wavelet is conceptually simple, memory efficient and computationally cheap. The haar transform also, does not have overlapping windows. Its formula is the following:

$$\phi(t) \begin{cases} 1, & \text{if } 0 \leq t \leq 1 \\ 0, & \text{otherwise} \end{cases}$$

If we define the function  $\psi(t)$  as  $\psi(t) = \phi(2t) - \phi(2t - 1)$ , we can obtain the following function:

$$\psi(t) = \begin{cases} 1, & \text{if } 0 < t \leq \frac{1}{2} \\ -1, & \text{if } \frac{1}{2} < t \leq 1 \\ 0, & \text{otherwise} \end{cases}$$

The function  $\phi(t)$  is the Haar scaling function, and  $\psi(t)$  is the Haar wavelet. [38]

### 2.5.7 Feature extraction in current work

In Fig. 2.11 we show that before proceeding with the preprocessing of the former matrix we created, we discard the time vector as we are not going to use the timestamps. Subsequently, we extract each 128-row-size segment from the matrix and we filter it with each feature we selected. After the feature extraction of each segment we convert the resulting matrix into a row. Each row represents the matrix from a preprocessed 128-row-size segment. The produced number of columns is variable for each different feature. We repeat all the aforementioned processes, for the data which are included in each of the folds.

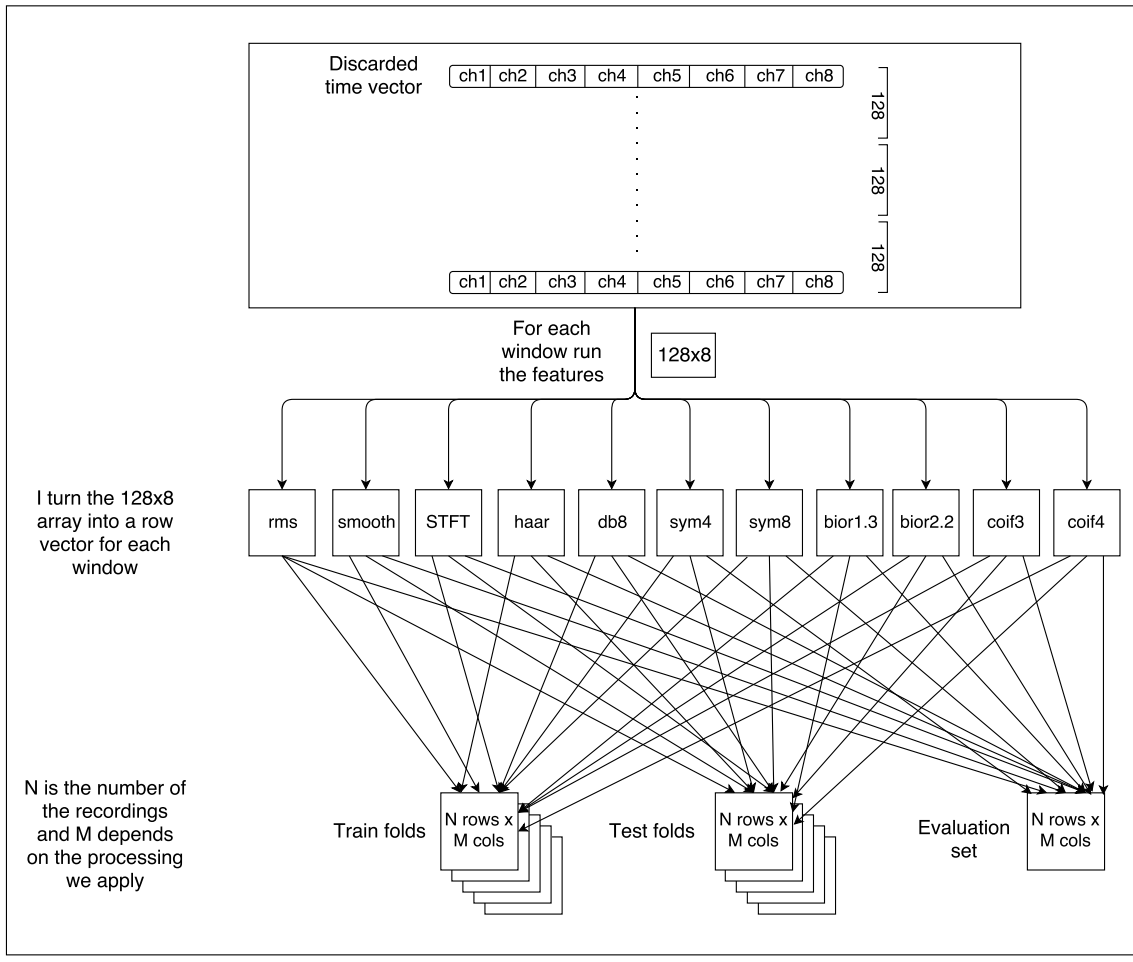


**Figure 2.11** Feature extraction

## 2.6 Training and classification

In Fig.2.12 we see that for each movement for feature from the train folds we train the SVM, ANN classifiers. After the training has happened we use the test folds we previously created and we classify them with the newly trained network. After, that classification we calculate the accuracy which is calculated by the extraction of mean-squared-error from one.

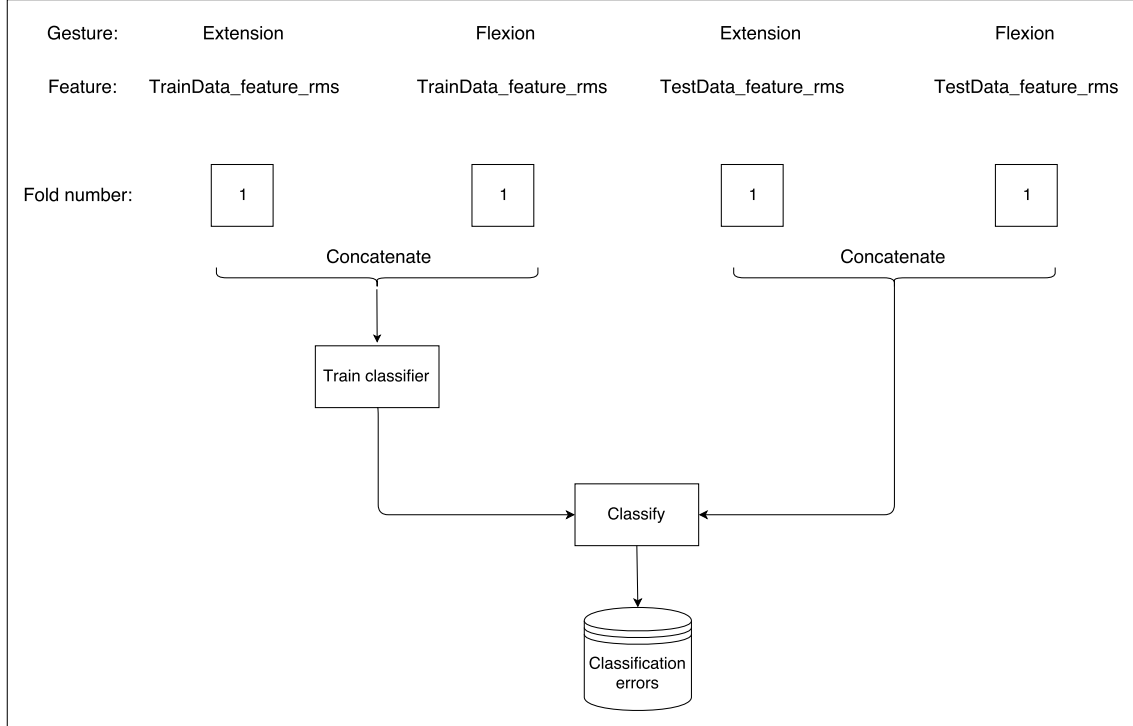


**Figure 2.12** Training & classification: For the training part we concatenate the n-th training fold with the extension and the flexion data for each of the extracted features. We proceed by training the model with these data. Then, we concatenate the n-th test fold for the extension and flexion data and for the same feature as we did for the training folds. After testing the newly trained neural network with the test data we have the detection accuracies.

### 2.6.1 Forward selection, backward elimination

A common problem in pattern classification is to select a subset of features from a pool of many potential variables. As in most cases, in ours too, data acquisition process collects samples on a large number of variables because it is unknown which ones are the most important for class discrimination. To identify and select the most important and nonredundant variables from the large pool of potential variables is the goal of the feature subset selection [41].

In the work of Jovic et al. forward selection typically starts with an empty feature set and then considers adding one or more features to the set [42].

In backward elimination, we typically start with the whole feature set and consider removing one or more features from the set.

Bidirectional search start from both sides, from an empty set and from the whole set, simultaneously considering larger and smaller feature subsets. Heuristic selection generates a starting subset based on a heuristic and then explores it further.

## 2.7 Artificial intelligence

Artificial intelligence (Artificial Intelligence (AI)) is a thriving field with many practical applications and current active research topics. AI tries to automate routine labor, understand speech or images, make diagnoses in medicine and support scientific research with the creation of intelligent software [43].

Artificial intelligence rapidly tackled and solved problems that are difficult for human beings but relatively straight-forward for computers, problems that can be described by a list of mathematical formulas. The demanding challenge for artificial intelligence is to solve tasks that are easy for people to solve but hard for them to describe formally, problems that we solve intuitively such as recognizing faces [43].

Computers have been able to defeat the best human chess players but only recently to recognize object or speech. A life of a person demands an immense amount of world knowledge. Much of this knowledge is subjective and therefore difficult to formally articulate. Thus, one of the key challenges in artificial intelligence is how to transfer this informal knowledge into the computer [43].

One solution is to create a knowledge base where we have to hard-code knowledge about the world formally. That will make the computer able to reason automatically about statements in languages that are designed to be used with logical inference rules. The disadvantage is that people struggle to describe everything about the world formally with logical rules [43].

This main disadvantage suggest that AI systems need the ability to acquire their own knowledge, by extracting patterns from data. This capability is also known as **machine learning**. The introduction of machine learning enable the computers to overcome problems that require knowledge of the real world and make decisions that appear subjective[43].

Many artificial intelligence tasks can be solved by finding the right set of features to extract for that task, then providing these features to a simple machine learning algorithm such as logistic regression or naive Bayes. Although, for many tasks, is difficult to know what features should be extracted.

A way to improve machine learning with feature extraction is to use machine learning to discover the representation itself. This is known as representation learning. With this approach, the AI systems are enabled to adapt to new tasks faster with minimal human intervention. A representation learning algorithm can discover a good set of features for a complex task requires hours to months whereas the same complex task would require a great deal of time and effort.

### 2.7.1 Biological and artificial neural networks

The human brain is the most complex and most powerful organ of the human body. The inner functionality of the human brain is modeled around the *neurons* and the

networks of neurons known as *biological neural networks*. The estimated number of human brain neurons is 100 billion, which are interconnected and communicate with one another through an interface consisting of *axon terminals* that are connected to *dendrites* across a gap (synapse) as shown in Fig. 2.13. Simply put, the neuron

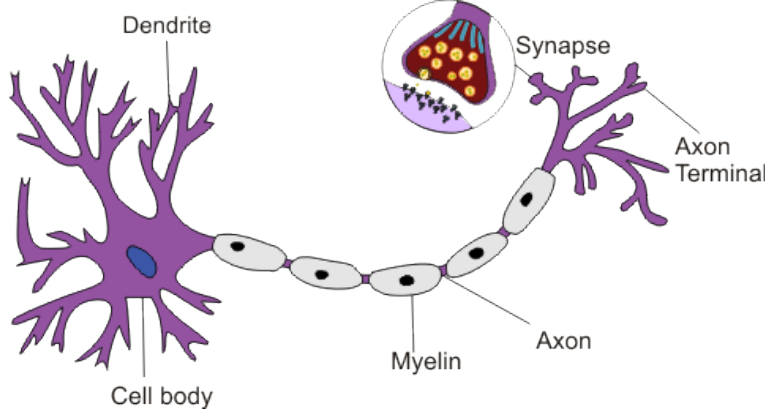


**Figure 2.13** Anatomy of a biological neuron [44]

will pass a message to another neuron across this interface if the sum of weighted input signals from one or more neurons exceeds a threshold to cause the message transmission. When the threshold is exceeded and the message is passed along to the next neuron is known as *activation*.

An artificial neural network is basically a mathematical function. It is built from simple functions which have parameters which get adjusted. An example of such a function is shown in Fig. 2.14. The below network takes  $x_1$  to  $x_n$  as numerical inputs and has weights  $w_1$  to  $w_n$  associated with these inputs. Additionally, there is another input 1 with bias  $b$  (called the bias) associated with it. There are thousands of those simple functions (also called “neurons”) which build an artificial neural network. Each neuron’s input signal is a weighted combination of many input signals and the weight of each input means that the input can have a different influence on any subsequent calculations, and ultimately on the final output of the entire network. In addition, the main function of bias is to provide every node with a trainable constant value in addition to the normal inputs that the node receives.

Additionally, each neuron applies a transformation function to the weighted inputs, meaning that the summed weighted input signal is transformed mathematically prior to evaluating only if the activation threshold is exceeded. Here we list some of the several activation functions someone can encounter in practice: log-sigmoid, tan-sigmoid, the positive linear often referred to as rectified linear unit (ReLU) and the softmax tranfer functions which we will explain them later in detail. The combination of the weighted of input signals and the functions applied are typically either linear or nonlinear.

These input signals can originate in many ways, with our senses being some of the most important, as well as breathing, drinking and eating for example. A single neuron can receive hundreds of thousands of these input signals at once that undergo the summation process to determine if the message gets passed along and ultimately causes the brain to instruct actions, memory recollection and so on.

All the thoughts which are generated in our brains and the subsequent instructions given to our muscles, organs, and body are the results of these neural networks in action. The brain’s neural networks continuously change and update themselves in

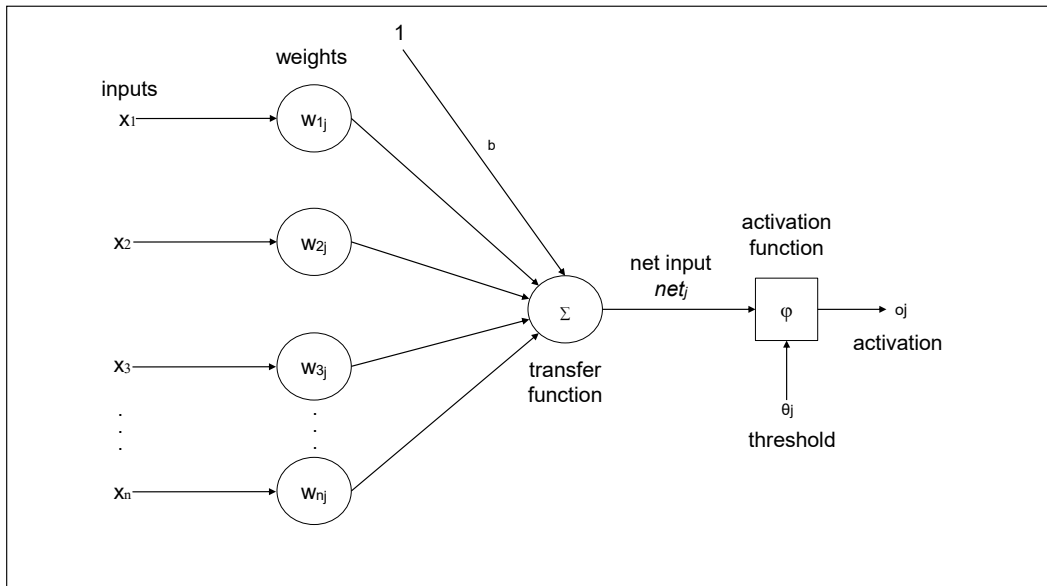


**Figure 2.14** Artificial neuron

many ways, including modifications to the amount of weighting applied among the neurons.

Ergo, it comes naturally to assume that, in order to transfer the brain's functionality and capabilities to a computing machine, it must be implemented by a computer, artificial version of this network of neurons. This is the birth of this statistical processor and known as *artificial neural networks*.

## 2.7.2 Artificial neural networks

Artificial neural network is an interconnected group of natural or artificial neurons that uses a mathematical or computational model inspired by and modeled on biological neural networks. They are capable of processing nonlinear relationships between inputs and outputs in parallel. These networks are characterized by containing adaptive weights along the paths of many neurons which can be tuned by a learning algorithm which learns from observed data in order to improve the model. Apart from the learning algorithm, a cost function has to be chosen.

The cost function is used to learn the optimal solution to the problem being solved. It helps in determining the best values for all the tunable parameters, by adapting the weights along with other parameters such as the learning rate. These values are determined through optimization techniques such as gradient descent or stochastic gradient descent. These optimization techniques try to find the optimal solution, which when successful that means that ANN is able to solve the problem in question with a high accuracy.

Architecturally, an artificial neural network is modeled using layers of artificial neurons, as shown in Fig. 2.14, which are able to receive input and apply an activation function along with a threshold to determine if messages are passed along.

As shown in Fig. 2.15 the first layer in a neural network model is always the input

layer followed by one hidden layer and lastly by an output layer. Each layer can contain one or more neurons. Models become increasingly complex by increasing the number of hidden layers, the number of neurons in any given layer or the number of paths between neurons. The following network is also known as feed-forward network.

Model architecture and tuning are therefore major components of ANN techniques

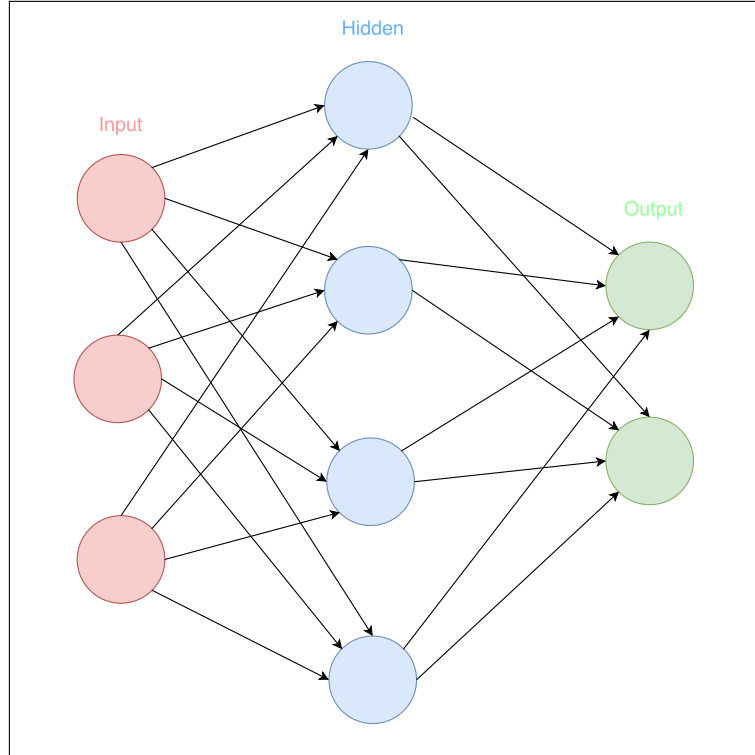


**Figure 2.15** Feed-forward network

in addition to the learning algorithms themselves. All of these characteristics of an ANN can have significant impact on the performance of the model. In addition, models are tuned by the activation function to convert a neuron's input to its output activation.

The meaning represented by a single artificial neuron is a form of local representation whereas the meaning of the entire neural network is a form of a distributed representation due to the accumulated transformations across the neurons and layers.

### 2.7.3 Deep learning

Many machine-learning systems nowadays make an extended use of a class of techniques called deep learning. Deep learning also known as deep structured learning, is a branch of machine learning based on a set of algorithms that attempt to model high level abstractions in data. In a simple single-layer network we could have two sets of neurons: ones that receive an input signal and ones that send an output signal. When the input layer receives an input it passes on a modified version of the input to the next layer. In a deep network, there are many layers between the input and the output, allowing the algorithm to use multiple processing layers, composed

of multiple linear and non-linear transformations. [43]

These methods have improved the state-of-the-art in speech recognition [45], object recognition [46] and in other domains such as drug discovery [47] and genomics [48]. The term “Deep Learning” was first introduced to machine learning by Dechter [49].

### 2.7.4 Deep learning architecture

We are going to list briefly the different deep learning architectures:

- **Generative deep architectures**, which are intended to characterize the high-order correlation of the observed or visible data for pattern analysis and characterize the joint statistical distributions of the visible data and their associated classes. [49] Some of the types of generative models are hidden markov model and restricted boltzmann machine.
- **Discriminative deep architectures**, which are intended to directly provide discriminative power for pattern classification, often by characterizing the posterior distributions of classes conditioned on the visible data. Some types of discriminative architecture are support vector machines, logistic regression which is a type of generalized of linear regression which is used for predicting binary or categorical outputs.
- **Hybrid deep architectures**, where the goal is discrimination but is assisted with the outcomes of generative architectures via better optimization and regularization, or discriminative criteria are used to learn the parameters in any of the deep generative models is the generative deep architectures category. [50]

### 2.7.5 Deep feed forward networks

Deep feed-forward networks, also called feed-forward neural networks, or multilayer perceptrons (Multilayer Perceptron (MLP)), are the quintessential deep learning models.

The goal of a feed-forward network is to approximate some function  $f^*$ . For example, for a classifier,  $y = f^*(x)$  maps an input  $x$  to a category  $y$ . A feedforward network defines a mapping  $y = f(x; \theta)$  and learns the values of the parameters  $\theta$  that result in the best function approximation.[43]

In simple terms, the network can be defined as input, hidden and output nodes with data coming in from input node, processing is done in hidden nodes and then the output is produced through the output nodes. The information flows through the function being evaluated from  $x$ , through the intermediate computations used to define  $f$ , and finally to the output  $y$ . There are no feedback connections in which outputs of the model are fed back into itself and hence the models is called as feed-forward network. When feedforward neural networks are extended to include feedback connections, they are called recurrent neural networks. These kind of networks are used in many natural language applications [51]. The convolutional networks which are used for object recognition from photos are a specialized kind of

feedforward network.[43]

Deep feedforward networks also called **feedforward neural networks** or multi-layer perceptrons are the most important deep learning models. Feedforward neural networks are called networks because they are typically represented by composing together many different functions [43]. The model is associated with a directed acyclic graph describing how the functions are composed together. For example, we might have three functions  $f^{(1)}$ ,  $f^{(2)}$  and  $f^{(3)}$  connected in a chain, to form  $f(x) = f^{(3)}(f^{(2)}(f^{(1)}(x)))$ . These chain structures are the most commonly used structures of neural networks. In this case,  $f^{(1)}$  is called the first layer of the network,  $f^{(2)}$  is called the second layer, and so on. The overall length of the chain gives the depth of the model. The name “deep learning” arose from this terminology. The final layer of a feedforward network is called the output layer. During neural network training, we drive  $f(x)$  to match  $f^*(x)$ . The training data evaluate  $f(x)$  with noisy, approximate examples of  $f^*(x)$  at different training points. Each example  $x$  is accompanied by a label  $y \approx f^*(x)$ . The training examples specify directly what the output layer must do at each point  $x$ ; it must produce a value that is close to  $y$ . The learning algorithm must decide how to use those layers to produce the desired output, but the training data do not determine what each individual layer is expected to do. Instead, the learning algorithm must decide how to use these layers to best implement an approximation of  $f^*(x)$ . Because the training data does not show the desired output for each of these layers, they are called **hidden layers**. [43] As these networks are inspired by neuroscience these networks are called neural. Each hidden layer of the network is vector valued. The dimensionality of these hidden layers determines the width of the model. Each element of the vector can be interpreted as playing a role analogous to a neuron. Rather than thinking of the layers as representing a single vector-to-vector function, we can imagine the layer as consisting of many inputs that act in parallel, each representing a vector-to-scalar function. Each unit resembles a neuron in the sense that it receives input from many other units and computes its own activation value. The idea of using many layers of vector-valued representations is originating from neuroscience. The choice of the functions  $f^{(i)}(x)$  used to compute these representations is also guided by neuroscientific observations about the functions that biological neurons compute. It is best to think of feedforward networks as machines that try to approximate functions which are designed to achieve statistical generalization. [43]

Linear models can help us to find a way to understand feedforward networks. Linear models such as logistic regression and linear regression, are appealing because they can be fit efficiently and reliably. Linear models also have the obvious defect that the model is limited to linear functions, so the model cannot understand the interaction between any two input variables.

To represent nonlinear functions of  $x$ , we can apply the linear model not to  $x$  itself but to a transformed input  $\phi(x)$ , where  $\phi$  is a nonlinear transformation. We can think of  $\phi$  as providing a set of features describing  $x$ , or as providing a new representation for  $x$ . The question arises on how to choose the mapping  $\phi$ .

- One option is to use a generic  $\phi$ . If  $\phi(x)$  has high dimension, we can have enough capacity to fit the training set, but generalization to the test set remains poor. Very generic feature mappings are usually based only on the principle of local smoothness and do not encode enough prior information to solve advanced problems. [43]

- Another way is to manually configure  $\phi$ . Till the advent of deep learning, this was the dominant approach. It requires a lot of human effort for each separate task, with practitioners in different domains, such as speech recognition or computer vision.[43]
- The strategy of deep learning is to learn  $\phi$ . In this approach, we have a model  $y = f(x; \theta, w) = \phi(x; \theta)^T w$ .  $\theta$  parameter is used to learn  $\phi$  from a broad class of functions, and parameter  $w$  that map from  $\phi(x)$  to the desired output. This is an example of a deep feedforward network, with  $\phi$  defining a hidden layer. In this approach, we parameterize the representation as  $\phi(x; \theta)$  and use the optimization algorithm to find the  $\theta$  that corresponds to a good representation. The advantage with this approach is that the human designer only needs to find the right general function family rather than finding precisely the right function. [43]

The general principle of improving models by learning features extends beyond the feedforward networks. Feedforward networks are the application of this principle to learnings deterministic mapping from  $x$  to  $y$  that lack feedback connections. Other models, apply these principles to learning stochastic mappings, functions with feedback and probability distributions over a single vector. [43]

Last but not least, feedforward networks have introduced the concept of hidden layer, and this requires us to choose the activation functions that will determine the hidden layer values. We should also take into consideration about how many layers the network should contain, how these layers should be connected to each other and how many units should be in each layer. Learning in deep neural networks requires computing the gradients of complicated functions. The back-propagation is one of these algorithms which are used to compute these gradients.

### 2.7.6 Learning Conditional Statistics

Instead of learning a full probability distribution  $p(y|x; \theta)$ , we want to learn just one conditional statistic of  $y$  given  $x$ . For example, we may have a predictor  $f(x; \theta)$  that we wish to employ to predict the mean of  $y$ . From this point of view, we can view the cost function as being a functional rather than just a function. A functional is a mapping from functions to real numbers. Therefore, we can think of learning as choosing a function rather than merely choosing a set of parameters. For example, we can design the cost functional to have its minimum lie on the function that maps  $x$  to the expected value of  $y$  given  $x$ . To solve the optimization problem with respect to a function requires a mathematical tool called **calculus of variations**. [52] Our first result derived using calculus of variations is that solving the optimization problem

$$f^* = \operatorname{argmin} \mathbb{E}_{x,y \sim p_{\text{data}}} \|y - f(x)\|^2 \quad (2.7)$$

yields

$$f^*(x) = \mathbb{E}_{y \sim p_{\text{data}}(y|x)}[y] \quad (2.8)$$

so long as this function lies within the class we optimize over. To put it simply, if we could train on infinitely many samples from the true data generating distribution,

minimizing the mean squared error cost function would give a function that predicts the mean of  $y$  for each value of  $x$ .

Different cost functions give different statistics. A second result derived using calculus of variations is that:

$$f^* = \operatorname{argmin} \mathbb{E}_{x,y \sim p_{\text{data}}} \quad (2.9)$$

yields a function that predicts the median values of  $y$  for each  $x$ , as long as such a function may be described by the family of functions we optimize over. This cost function is commonly called **mean absolute error**.[43]

### 2.7.7 Common Activation Functions

When we construct an ANN model, one of the main consideration is to choose the proper activation function for hidden and output layers that are differentiable. The main reason behind that, is that when we calculate the backpropagated error signal that is used to determine ANN parameter updates requires the gradient of the activation function gradient. Four of the most common functions and their associated gradients are plotted in Fig.2.16 :

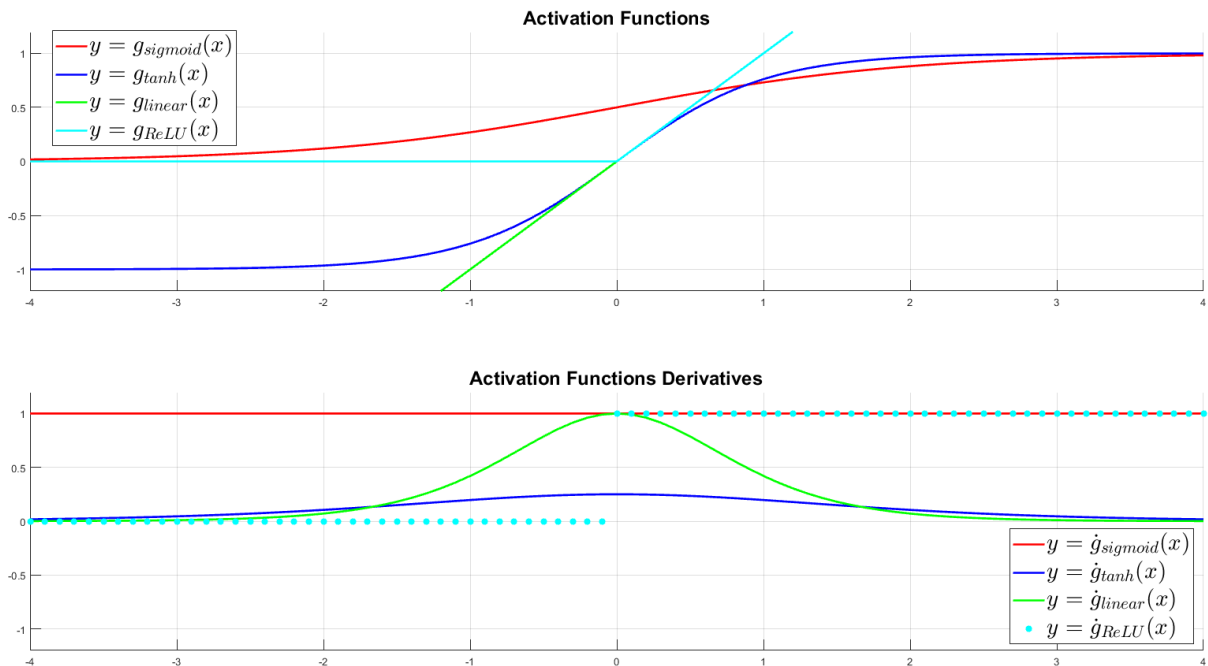


**Figure 2.16** Common activation functions used in artificial neural networks along with their derivatives.

## 2.7.8 Identity Activation Function

The simplest activation function, that is commonly used for the output layer in regression problems, is the identity/linear activation function:

$$g_{\text{linear}}(z) = z$$

This activation function maps the pre-activation to itself and can output values that range  $(-\infty, \infty)$ . Even though, a multi-layered network with linear activations at each layer can be equally formulated as a single-layered linear network, the identity activation function seems to be extremely useful. In the case, where a multi-layered network that has nonlinear activations functions amongst the hidden units and an output layer that uses the identity activation function implements a powerful form of nonlinear regression. [43]

## 2.7.9 Logistic Sigmoid

A function that is often used as the output activation function for binary classification problems is the logistic sigmoid. The logistic sigmoid has the following form:

$$g(z) = \sigma(z) = \frac{1}{1 + e^{-z}} \quad (2.10)$$

and output values that range  $(0, 1)$ . The logistic sigmoid can be interpreted as the probability of an artificial neuron “firing” given its inputs. Calculating the derivative of the logistic sigmoid makes use of the quotient rule:

$$\begin{aligned} g'_{\text{logistic}} &= \frac{\partial}{\partial z} \left( \frac{1}{1 + e^{-z}} \right) \\ &= \frac{e^{-z}}{(1 + e^{-z})^2} \\ &= \frac{1 + e^{-z} - 1}{(1 + e^{-z})^2} \\ &= \frac{1 + e^{-z}}{(1 + e^{-z})^2} - \left( \frac{1}{1 + e^{-z}} \right)^2 \\ &= \frac{1}{(1 + e^{-z})} - \left( \frac{1}{1 + e^{-z}} \right)^2 \\ &= g_{\text{logistic}}(z) - g_{\text{logistic}}(z)^2 \\ &= g_{\text{logistic}}(z)(1 - g_{\text{logistic}}(z)) \end{aligned} \quad (2.11)$$

This turns out to be convenient as we can see that  $g'_{\text{logistic}}(z)$  evaluated at  $z$  is  $g_{\text{logistic}}(z)$  weighted by  $1 - g_{\text{logistic}}(z)$  thus the gradients for the layers can be evaluated using simple multiplication and subtraction rather than performing any re-evaluating the sigmoid function, which requires extra exponentiation.

## 2.7.10 Hyperbolic Tangent

Although the logistic sigmoid has a biological interpretation, it turns out that the logistic sigmoid can cause a neural network to get “stuck” during training. In the case

where a strongly-negative input is provided to the logistic sigmoid, it output values very near to zero. As we know, neural networks use the feedforward activations to calculate parameter gradients this affect the model parameters that are updated less regularly than we would like and thus they are stuck in their current state.[43]

An alternative to the logistic sigmoid is the hyperbolic tangent, or tanh function:

$$\begin{aligned} g_{tanh}(z) &= \frac{\sinh(z)}{\cosh(z)} \\ &= \frac{e^z - e^{-z}}{e^z + e^{-z}} \end{aligned} \tag{2.12}$$

As the logistic sigmoid, the tanh function is also sigmoidal but instead outputs values that range  $(-1, 1)$ . Thus strongly negative inputs to the tanh will map to negative outputs. Additionally, zero-valued inputs are mapped to near-zero outputs. These properties make the network less likely to get “stuck” during training. Calculating the gradient for the tanh function also uses the quotient rule:

$$\begin{aligned} g'_{tanh}(z) &= \frac{\partial}{\partial z} \frac{\sinh(z)}{\cosh(z)} \\ &= \frac{\frac{\partial}{\partial z} \sinh(z) \cosh(z) - \frac{\partial}{\partial z} \cosh(z) \sinh(z)}{\cosh^2(z)} \\ &= \frac{\cosh^2(z) - \sinh^2(z)}{\cosh^2(z)} \\ &= 1 - \frac{\sinh^2}{\cosh^2} \\ &= 1 - \tanh^2(z) \end{aligned} \tag{2.13}$$

Similar to the derivative for the logistic sigmoid, the derivative of  $g_{tanh}(z)$  is a function of feedforward activation evaluated at  $z$ , namely  $(1 - g_{tanh}(z)^2)$ .

### 2.7.11 Rectified Linear Units

Rectified linear units use the activation function  $g(z) = \max\{0, z\}$ . These units are easy to optimize because they are similar to linear units. The only difference between a linear unit and a rectified linear unit is that a rectified linear unit outputs zero across half its domain. Therefore, this makes the derivatives through a rectified linear unit remain large whenever the unit is active. The gradients are not only large but also consistent. The second derivative of the rectifying operation is 0 almost everywhere, and the derivative of the rectifying operation is 1 everywhere the unit is active.[43]

Rectified linear units are typically used on top of an affine transformation:

$$h = g(W^T x + b) \tag{2.14}$$

When initializing the parameters of the affine transformation, it can be a good practice to set all elements of  $b$  to a small positive value, such as 0.1. By doing so, it will be most likely that the rectified linear units will be active for most inputs in the training set and allow the derivatives to pass through.

When using a neural network to approximate a function, the data is forwarded through the network layer by layer until it reaches the final layer. The final layer's activations are the predictions that the network outputs. The essence of training our model is to find the right set of weights for all the connections to make the right decision. To measure how well is our model performing we determine a metric which is also known as cost function. The discrepancies between the outputs in the estimations and the training set data are the principle values for our cost function. The goal of the training is to get the value of this cost function as low as possible.[43]

### 2.7.12 Softmax function

The softmax transfer function is typically used as the transfer function for the output layer. It divides each output such that the total sum of the outputs is equal to one. The softmax function computes a categorical probability distribution that tells the probability that any of the classes are true. The mathematical formula for the softmax function is the following:

$$f(z)_i = \frac{e^{z_i}}{\sum_{j=1}^c e^{z_j}} \quad (2.15)$$

In the above equation  $z$  is a vector of the inputs to the output layer and  $i$  indexes the output units.

### 2.7.13 Minimization of the cost function

One of the mostly used cost function is that of Mean-Squared-Error (Mean Squared Error (MSE)) and we denote is as  $J(W)$ .

$$J(W) = \frac{1}{m} \sum_{i=1}^m (h_W(x^{(i)}) - y^{(i)})^2 \quad (2.16)$$

where  $m$  is the number of training examples,  $x^{(i)}$  is the input vector for the  $i^{th}$  training example and  $y^{(i)}$  is the class label for the  $i^{th}$  training example and  $W$  are the chose parameter values or weights. Last but not least,  $h_W(x^{(i)})$  is the algorithm's prediction for the  $i^{th}$  training example using the parameters  $W$ .[53]

We need to find the proper weights that will make the score of this cost function as low as possible. Simply put we want to  $J(W)_{\mathbf{W}}$ . To successfully minimize this function we need to take the first derivative and set it to zero and solve, which eventually will give us the locations of every minimum/maximum in this function. However, there are some difficulties with this approach:

- The cost function often is complex, so computing an expression for its derivative is time and resource consuming.
- The cost function is also multi-dimensional and the need to find the points where all of those derivatives are zero is not trivial.

- There is a large number of minima and maxima throughout the function and sorting out which one is the one we should be using is also computationally expensive.

In addition to the aforementioned problems, as the size of networks begins to scale up, solving for the weights directly becomes increasingly infeasible. We overcome this problem by applying the so called iterative optimization algorithms which progressively work their way towards the optimal solution.

The most basic of the iterative optimization algorithms is the gradient descent. Generally, the cost function should be more or less convex, as Fig. 2.17 shows. To be truly convex however it is almost impossible. For the sake of simplicity, we need this example in order to explain how gradient descent works.

We start off by initializing our weight randomly, which puts us at the red as the Fig. 2.17 shows. Taking the derivative, we see the slope at this point is a large positive

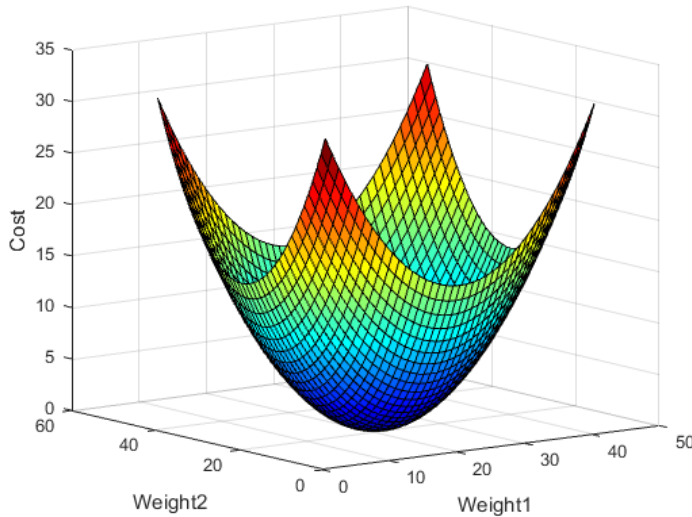


**Figure 2.17** Convex function  $z = x^2 + y^2$

number. Thus, we want to move closer to the center therefore we should take a large step in the opposite direction of the slope. If we repeat this process, eventually we will find the minimum of the curve as shown in Fig. 2.18 and much closer the optimal weight configuration for our model. The formula of gradient descent is as follows:

$$W := W - \alpha \frac{\partial J}{\partial W} \quad (2.17)$$

where  $\alpha$  is a parameter called the learning rate. For example, we assume that we have as a cost function  $J(W) = W^2$ . We want to find the value of  $W$  which minimizes  $J(W)$ . Let's assume that we start with  $W = 3$  and  $\alpha = 0.1$ . By doing simple calculations the Table 2.1 expresses how the value of  $J'(W) = 2W$  changes and approaches to zero. As can be seen in our simple example, every time the weights are updated, there is a subtraction of the cost function with respect to the weight scaled by the learning rate  $\alpha$ . Thus, leads to the derivative term getting smaller and smaller and converging near to zero. Also, selecting the right learning rate is critical. If the learning rate is too large, we can overstep the minimum and diverge.

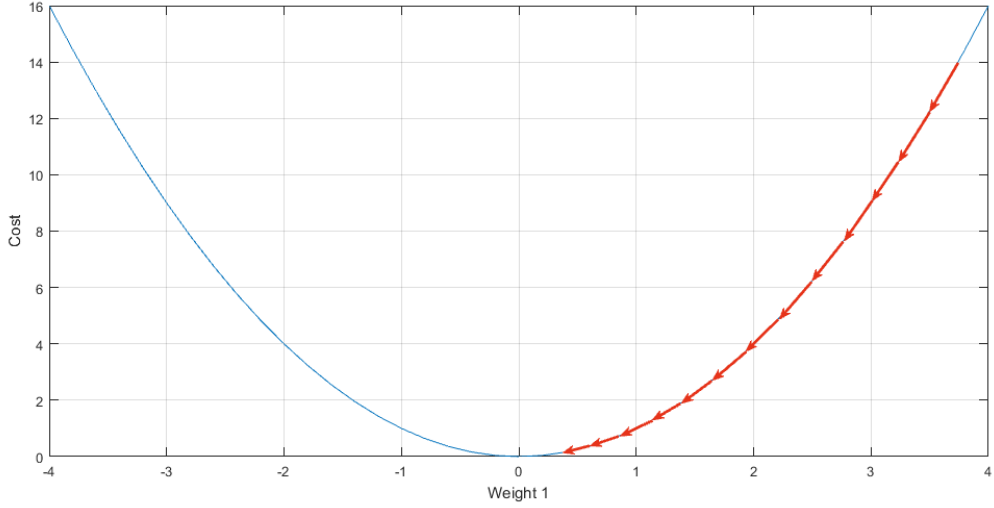


**Figure 2.18** Convex function  $y = x^2$

Iteration	$W$	$\alpha \frac{\partial J}{\partial W}$
1	3	0.6
2	2.4	0.48
3	1.92	0.384
4	1.536	0.307
5	1.229	0.246
6	0.983	0.197
7	0.786	0.157
8	0.629	0.126
9	0.503	0.101
10	0.403	0.081

**Table 2.1** The values of  $W$  prior to each iteration and the update amounts.

On the contrary, if we choose a too small value for the learning rate we need to run more iteration of gradient descent and this will lead to the increase of the training time [53].

In the above example we examined the case of a single variable cost function. Additionally to the single variable cost function we can have two or more variables in the cost function. Let's examine the case of the function  $J(W) = W_1^2 + W_2^2$ . This convex function is shown in Fig. 2.17. When there are multiple variables in the minimization objective, gradient descent defines a separate update rule for each variable. Let's try to show mathematically how the derivatives of the cost functions build up:

$$\begin{aligned}\frac{\partial}{\partial W_1} J(W_1, W_2) &= \frac{\partial}{\partial W_1} W_1^2 + \frac{\partial}{\partial W_1} W_2^2 = 2W_1 \\ \frac{\partial}{\partial W_2} J(W_1, W_2) &= \frac{\partial}{\partial W_2} W_1^2 + \frac{\partial}{\partial W_2} W_2^2 = 2W_2\end{aligned}$$

As we can see, when we take the partial derivative with respect to  $W_1$  we treat  $W_2$  as a constant.

We showed the MSE cost function in Eq. 2.16. Similarly, with the previous derivatives let's develop the derivative of the MSE cost function:

$$\begin{aligned}\frac{\partial}{\partial W_0} J(W_0, W_1) &= \frac{\partial}{\partial W_0} \left( \frac{1}{m} \sum_{i=1}^m (h_W(x^{(i)}) - y^{(i)})^2 \right) \\ &= \frac{1}{m} \sum_{i=1}^m \frac{\partial}{\partial W_0} (h_W(x^{(i)}) - y^{(i)})^2 \\ &= \frac{1}{m} \sum_{i=1}^m 2(h_W(x^{(i)}) - y^{(i)}) \frac{\partial}{\partial W_0} (h_W(x^{(i)}) - y^{(i)}) \\ &= \frac{2}{m} \sum_{i=1}^m (h_W(x^{(i)}) - y^{(i)})\end{aligned}$$

Lastly, each update of the  $W$  variables is averaged over the training set. Every training example suggests its own modification to the weight values and then we average these suggestions to make our actual update. This means that the statistics of our training set are being taken into account during the learning process. An outlier training example (mislabeled or corrupted one) is going to have less influence over the final weights. [53]

## 2.7.14 Backpropagation

Before the backpropagation algorithm there were many other methods implemented to adjust the weights in a random, uninformed direction (ie. increase or decrease) and check if the performance of the ANN is increasing. If it did not increase, then one would attempt to either go in the other direction or reduce the perturbation size or combine both [54].

Backpropagation give us an understanding on how to change the weights and biases in a network to have the desired changes on the cost function. For other machine learning algorithms like logistic regression (the sigmoid function) or linear regression computing the derivatives is an elementary application of differentiation. The same, however, cannot be said for neural networks. To demonstrate this, we will demonstrate a diagram of a double-layered neural network: In Fig. 2.19 we see that each neuron

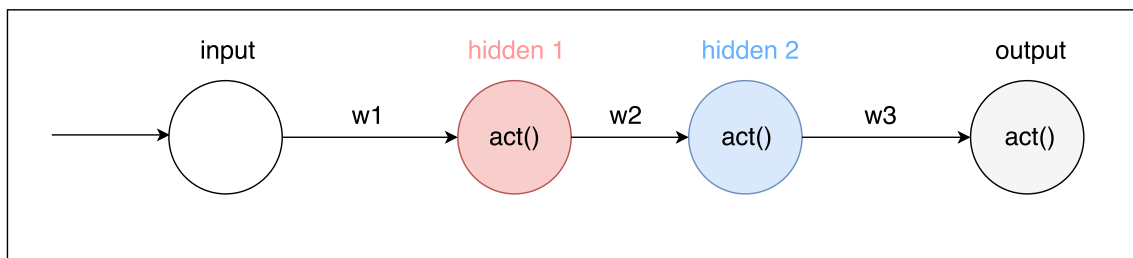


**Figure 2.19** Double layered neural network

is dependent of the previous one connected to it. Put it simply, if we change the

value of  $w_1$ , both “hidden 1” and “hidden 2” neurons (output layer inclusive) neurons will change. So we have the composite functions to compose the output function:

$$\begin{aligned} \text{output} &= \text{act}(w3 * \text{hidden2}) \\ \text{hidden2} &= \text{act}(w2 * \text{hidden1}) \\ \text{hidden1} &= \text{act}(w1 * \text{input}) \end{aligned}$$

Therefore we have:

$$\text{output} = \text{act}(w3 * \text{act}(w2 * \text{act}(w1 * \text{input}))) \quad (2.18)$$

As we see, the output is a composite function of the weights, inputs and activation functions. Now, let’s calculate the derivative of this function with respect to the arbitrary weight for example  $w_1$ . For this we have to apply the chain rule and we will have the following equation:

$$\frac{\partial}{\partial w1} = \frac{\partial}{\partial \text{hidden2}} \text{output} * \frac{\partial}{\partial \text{hidden1}} \text{hidden2} * \frac{\partial}{\partial w1} \text{hidden1}$$

If we are to compute the derivative of the error with any arbitrary weight the result equation will be:

$$\frac{\partial \text{error}}{\partial w1} = \frac{\partial \text{error}}{\partial \text{output}} * \frac{\partial \text{output}}{\partial \text{hidden2}} * \frac{\partial \text{hidden2}}{\partial \text{hidden1}} * \frac{\partial \text{hidden1}}{\partial w1}$$

Each of these derivatives can be simplified once we choose an activation and error function as we discussed earlier. At this point, any abstraction has been removed, and the error derivative can be used in gradient descent to iteratively improve upon the weight. We compute the error derivatives according to every other weight in the network and apply gradient descent similarly. This procedure is called the backpropagation where the computation of the derivatives are fed to an optimization algorithm. The name backpropagation justifies the whole procedure as we are traversing from the output error to the weights, taking iterative steps using the chain rule until we reach the weight [54].

### 2.7.15 Summary of training neural network

We can summarize the steps of training an entire neural network:

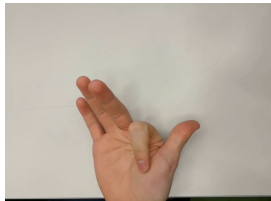
1. Create our connected neural network and prepare training data
2. Initialize all the weights to random values. Here we have to emphasize we must not initialize the weights to zero. If weights are initialized to zero, the outgoing weights of each neuron will be identical because the gradients will be identical. Due to this, the proceeding hidden neurons will keep the same value and will continue to follow each other. This means that our neural network may get stuck at local optima. Therefore, random weight initialization allows us to overcome this problem by starting with many random values.[54]
3. Perform one feed-forward using the training data

4. Perform backpropagation to get the error derivatives for each and every weight in the neural network
5. Perform gradient descent to update each weight of the respective error derivative.
6. If we have converged training is complete. In reality most time, we stop when we have reached the number of maximum iterations.

## 2.8 Data evaluation

To test the optimal parameters for our neural network we need evaluation data. We created a new database with finger gestures consisted only from EMG signals. The signals were acquired with the Myo armband. The IMU data was discarded since there was no motion of the hand only motion of the fingers and keeping still the hand during the whole experiment. The 80% percent of the new acquired data was used to train the neural nets and the rest 20% was used to test the newly trained neural nets.

After the protocol for the new finger gestures was created and we created a database with the 14 new finger gestures and classify them into two classes: extension and flexion. We acquired new signals from the forearms of 21 subjects aged between 20-30. Below are the images with the extensions and the flexions of the gestures:



G1: Index extension and flexion with the palm facing upwards



G2: Index extension and flexion with the palm facing downwards



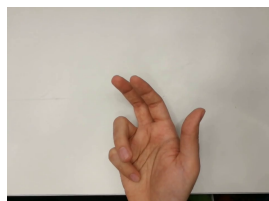
G3: Moving index finger from and to pair(middle,ring,pinky)



G4: Middle finger extension and flexion with the palm facing upwards



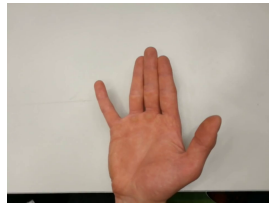
G5: Middle finger extension and flexion with the palm facing downwards



G6: Pinky finger extension and flexion with the palm facing upwards



G7: Pinky finger extension and flexion with the palm facing downwards



G8: Moving pinky finger from and to pair (ring, middle, index)



G9: Thumb finger extension and flexion with the palm facing upwards



G10: Thumb finger extension and flexion with the palm facing downwards

---



G11: Pairing and unpairing thumb with pinky



G12: Pairing and unpairing pair1(index, middle) with pair2(ring, pinky)



G13: Ring finger extension and flexion with the palm facing upwards



G14: Ring finger extension and flexion with the palm facing downwards

---

**Figure 2.21** 14 finger gestures from 21 different subjects were acquired using the Myo armband

---



# 3

## Results

In this chapter we will present the results coming from the process of parameter adjustment and the results coming from the final evaluation. During the parameter adjustment we use as an input for our neural network, EMG data with the Myo armband coming from the forearm regarding extension and flexion of the thumb. For the evaluation stage we acquired EMG signals from 21 subjects regarding extension and flexions of different gestures.

### 3.1 Parameter adjustment

The first experiment we ran had the purpose to find the best average accuracies for the detection between thumb extension and flexion per feature. As fig. 3.1 shows, we have estimated the average accuracies for the training and testing of each of the 55 folds of data we have created. The best accuracy was from the discrete wavelet bior1.3 which gave 64% detection accuracy and the worst performance was from the root-mean-square with 53.1%.

The time for training the model and testing it for the existing amount of data has found to be prohibitively long. Therefore, due to the large quantity of data we chose for the next experiments to decrease the amount of it by increasing the step of the windowing from 1 to 64. The second experiment had the purpose to check whether the neural net with one hidden layer and five hidden nodes can give us similar or better results with less data. Fig. 3.2 shows slightly better results than the first batch. As we can observe in almost every feature we got better results with less data.

For the next experiment we decided to combine all possible combinations of the train and test data extracted with the window step of 64 produced from the different features we selected for the current work. In total, we have 11 features and each feature has five folds for the training data and five folds for the test data. Combining

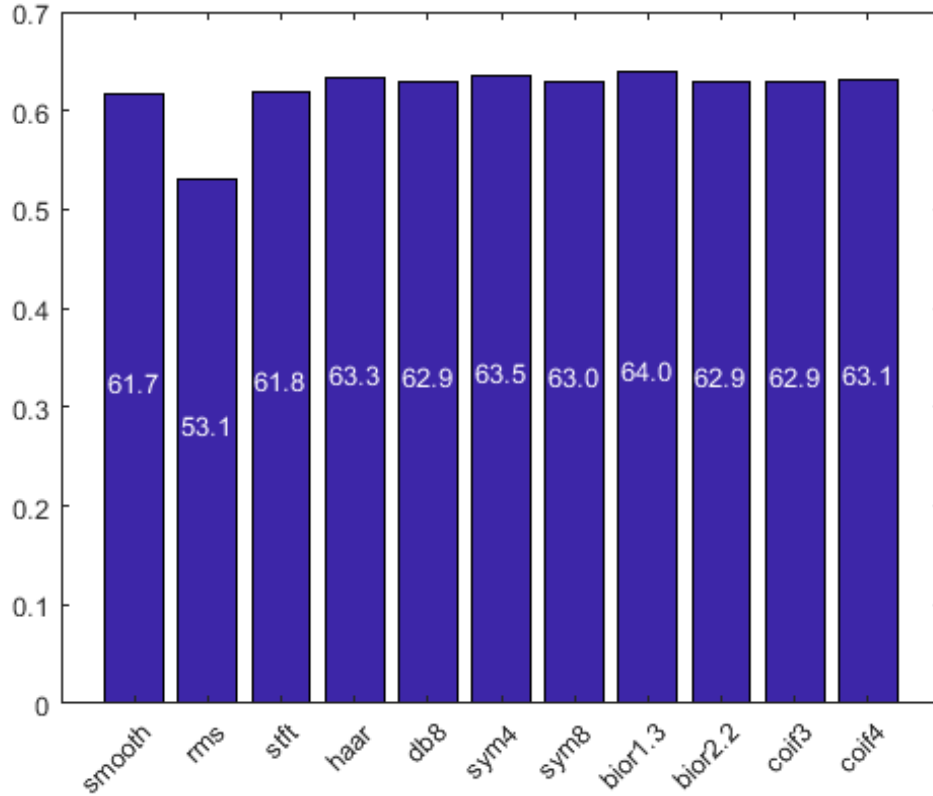


**Figure 3.1** Average performances with one hidden layer, five neurons and step one

all 11 features in groups of two then there are 55 combinations which is calculated by the following equation:

$$\binom{n}{k} = \frac{n(n-1)\cdots(n-k+1)}{k(k-1)\cdots 1} = \frac{n!}{k!(n-k)!} \quad (3.1)$$

Taking into account that each combination is accompanied by five folds of training and test data it means that we will run  $55 \times 5 = 275$  neural nets. The overall runtime of the whole experiment was 5.8 days. The average time for one experiment was 30.7 minutes. In Table 3.1 we can see the results of the average detection accuracies between extension and flexion of the thumb from testing the trained neural nets with one hidden layer and five hidden neurons. The best performances are highlighted with blue color. From the Table 3.1 we can see that the best performance is when we combine the features sym4 with sym8. For the next step we decided to concatenate the sym4 with sym8 and combine their concatenation with each and every other feature from the feature set.

In Table 3.2 we can see the average performances per 3 features for classification in one hidden layer and five hidden neurons network. For the next experiment we chose the second best performance from the Table 3.1 which was between the rms and sym8. We concatenated the two features and again tested against every other feature. The Table 3.3 show us the results:

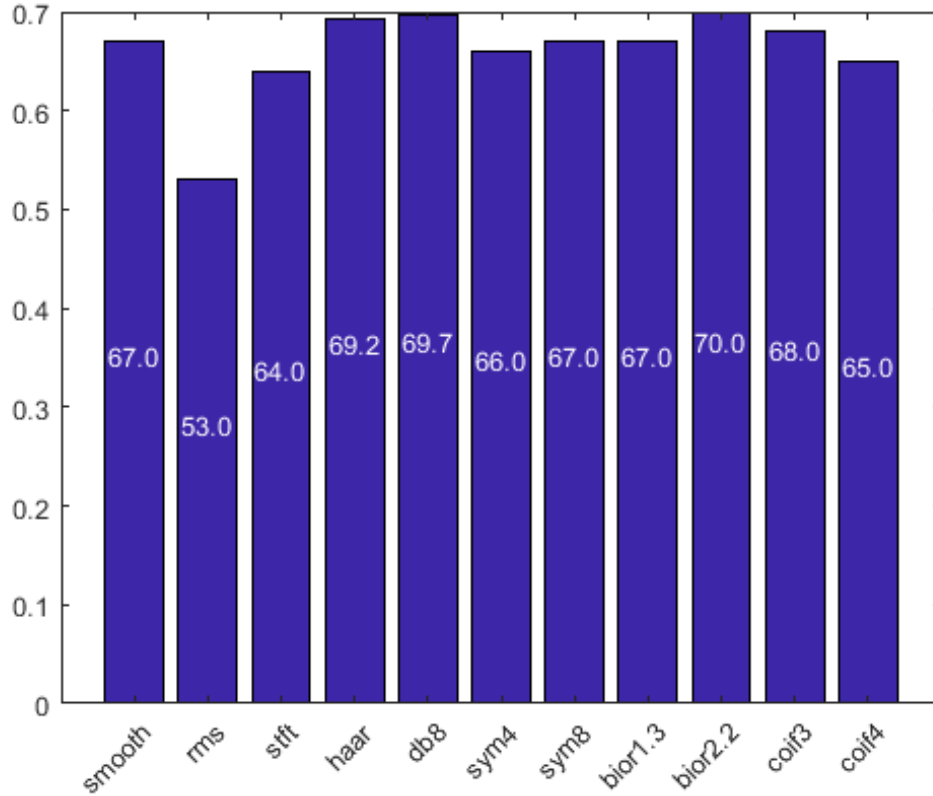


**Figure 3.2** Average performances with one hidden layer, five neurons and step 64

For the next experiment we chose the third best performance from the Table 3.1 which was between between the rms and bior1.3. Again, we concatenated these two features and tested against every other feature. The Table 3.4 show us the results: For the next experiment, we decided to concatenate the duplet of sym4 and sym8 and test it against all the other features and also incrementing the number of layers from one to eight layers with each consisting of 5 hidden neurons. The total number of nets that had to be trained was 585. The duration of this experiment was 73 days. The average time for each training and classification was 2.9 hours. The Table 3.5 shows us the results: Due to the time-consuming nature of the feature elimination process we decided to complete the experiments as we reached 13 layers in our neural network. Taking into account all the estimated average accuracies we plotted in 3 axes, the features according to their accuracies they had between each other in each layer. The following plot of the heatmap of the Table 3.5 is helping to give us a better visualization on which features had the best improvement over the increase of the layers of the neural networks.

## 3.2 Final evaluation

To conduct the final evaluation we take the best parameters derived from the previous experiments for the adjustment of the parameters.

As we can see 3.3 the rms feature does not perform so well as the other features. We will avoid to use 13 layers for our neural model as there is a risk of overfitting

Average accuracies from the combinations of all features										
Features	rms	stft	haar	db8	sym4	sym8	bior1.3	bior2.2	coif3	coif4
smooth	64.4%	63.0%	58.9%	65.4%	63.7%	67.1%	67.4%	65.3%	66.2%	69.3%
rms	-	66.1%	61.7%	69.2%	62.9%	69.9%	70.0%	63.1%	69.0%	68.0%
stft	-	-	67.0%	61.6%	66.3%	60.9%	68.8%	67.9%	62.4%	63.0%
haar	-	-	-	67.9%	66.9%	64.0%	66.3%	62.7%	63.1%	64.8%
db8	-	-	-	-	69.2%	66.7%	68.7%	59.5%	66.4%	65.8%
sym4	-	-	-	-	-	70.3%	68.2%	62.0%	67.8%	66.1%
sym8	-	-	-	-	-	-	66.8%	59.4%	64.2%	64.7%
bior1.3	-	-	-	-	-	-	-	66.8%	69.4%	59.5%
bior2.2	-	-	-	-	-	-	-	-	69.3%	65.7%
coif3	-	-	-	-	-	-	-	-	-	65.9%

**Table 3.1** Combined features and ran on neural net with one hidden layer and five hidden neurons.

Average accuracies from the combinations of all features										
Features	smooth	rms	stft	haar	db8	bior1.3	bior2.2	coif3	coif4	
sym4sym8	58.0%	61.0%	65.1%	65.2%	64.5%	65.7%	68.7%	68.4%	67.9%	

**Table 3.2** Combined features per 3 and ran on neural net with one hidden layer and five hidden neurons.

Average accuracies from the combinations of all features										
Features	smooth	stft	haar	db8	sym4	bior1.3	bior2.2	coif3	coif4	
rmssym8	58.1%	64.8%	59.7%	57.9%	62.1%	58.2%	62.0%	60.3%	63.3%	

**Table 3.3** Combined features per 3 and ran on neural net with one hidden layer and five hidden neurons.

Average accuracies from the combinations of all features										
Features	smooth	stft	haar	db8	sym4	sym8	bior2.2	coif3	coif4	
rmsbior1.3	61.9%	62.3%	65.8%	62.9%	61.8%	63.3%	62.9%	62.8%	64.8%	

**Table 3.4** Combined features per 3 and ran on neural net with one hidden layer and five hidden neurons.

the train data. As we can notice the plateau with the best performances happen for 8 layers. Therefore, this is the number we will use for the final neural model. The features we will choose for the feature extraction are going to be db8, bior2.2, coif3, as they are the features with the best performances for 8 layers. We will evaluate the new finger gestures with a neural model which will consist of 8 layers and will train it with the triplet of sym4 and sym8 and one of the following best performed features for 8 layers: db8, bior2.2 and coif3.

We acquired new signals from the forearms of 21 subjects with age between 20-30. The new finger gestures we classify are the following: The detection accuracies of

sym4sym8									
Layers	smooth	rms	stft	haar	db8	bior1.3	bior2.2	coif3	coif4
1 Layer	68.1%	61.0%	63.5%	67.0%	61.0%	68.0%	66.0%	64.4%	66.0%
2 Layers	69.7%	66.0%	70.5%	68.4%	69.2%	67.1%	69.5%	68.4%	67.0%
3 Layers	67.0%	63.7%	72.4%	70.0%	68.4%	71.2%	69.7%	69.1%	70.7%
4 Layers	72.0%	65.0%	71.4%	71.5%	72.1%	71.1%	70.5%	69.4%	73.0%
5 Layers	71.3%	67.8%	74.0%	72.5%	71.0%	71.5%	72.5%	70.5%	67.0%
6 Layers	74.2%	71.1%	73.0%	73.8%	74.2%	72.6%	74.1%	72.3%	71.5%
7 Layers	73.2%	68.6%	74.0%	73.5%	71.7%	73.0%	74.3%	73.8%	73.2%
8 Layers	72.9%	71.0%	72.3%	72.2%	73.5%	73.6%	73.5%	74.3%	72.0%
9 Layers	74.2%	63.2%	74.8%	72.8%	74.0%	73.5%	72.1%	74.4%	71.5%
10 Layers	73.0%	71.6%	73.8%	74.2%	72.3%	73.0%	74.1%	74.8%	73.4%
11 Layers	74.1%	71.8%	73.8%	74.0%	74.6%	73.7%	74.2%	73.7%	72.5%
12 Layers	73.3%	70.1%	74.1%	73.1%	74.3%	74.1%	74.4%	74.0%	74.8%
13 Layers	74.6%	70.0%	74.5%	73.7%	74.3%	74.9%	74.9%	74.8%	74.6%

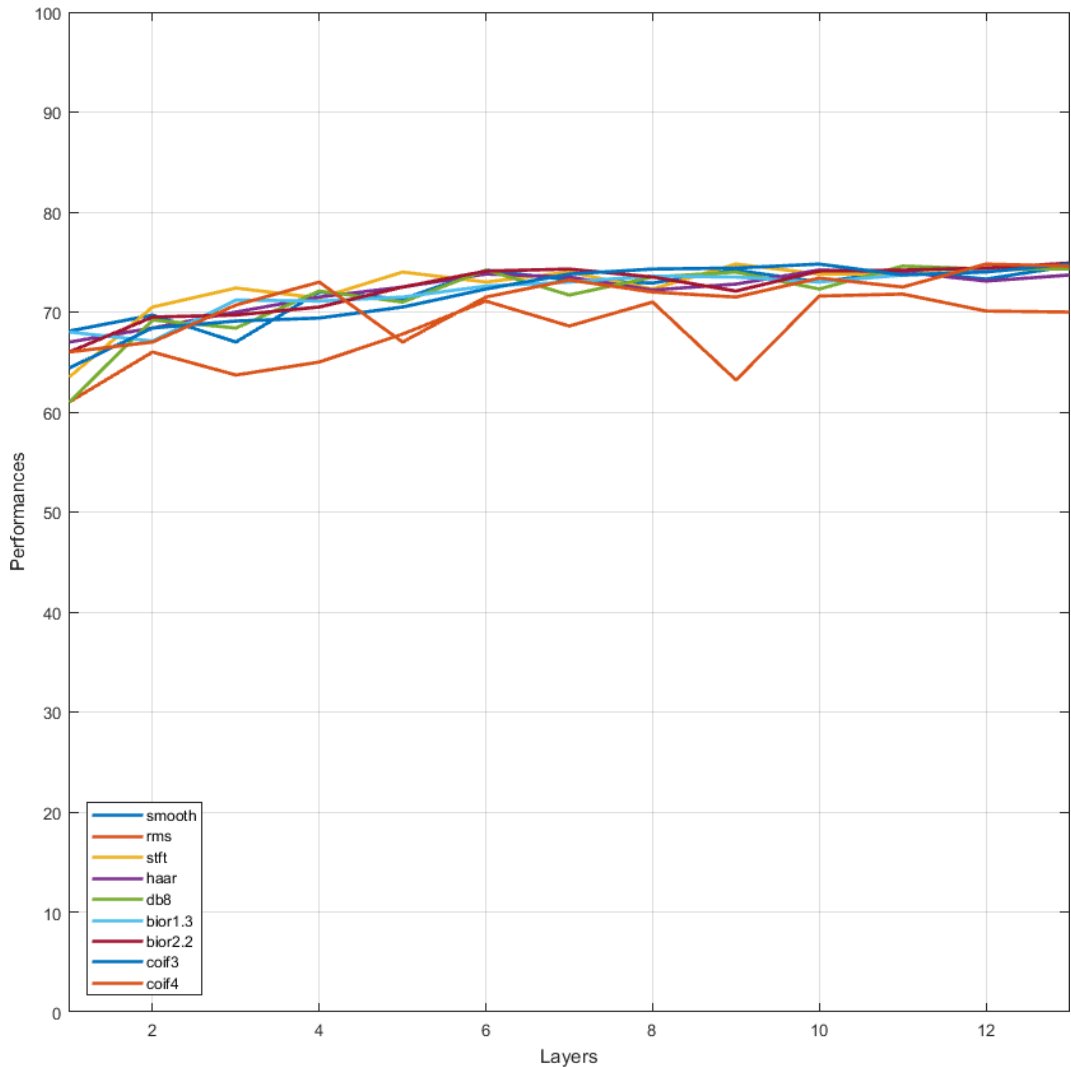
**Table 3.5** Best three performances per layer. Combined features per 3 and ran on neural net with incrementing the number of layers from one to eight.

the new gestures are listed below: The total number of neural nets that had to be

sym4sym8			
Gestures	db8	bior2.2	coif3
G1	64.5%	74.6%	50.1%
G2	73.7%	69.6%	62.7%
G3	68.8%	68.3%	66.1%
G4	58.2%	64.4%	62.6%
G5	58.1%	51.3%	52.0%
G6	74.5%	75.2%	72.0%
G7	54.4%	53.1%	56.0%
G8	63.8%	74.2%	62.7%
G9	62.8%	57.3%	70.0%
G10	61.8%	74.7%	65.0%
G11	73.1%	68.2%	70.0%
G12	55.7%	71.2%	52.2%
G13	63.5%	73.2%	67.6%
G14	54.8%	50.8%	73.0%

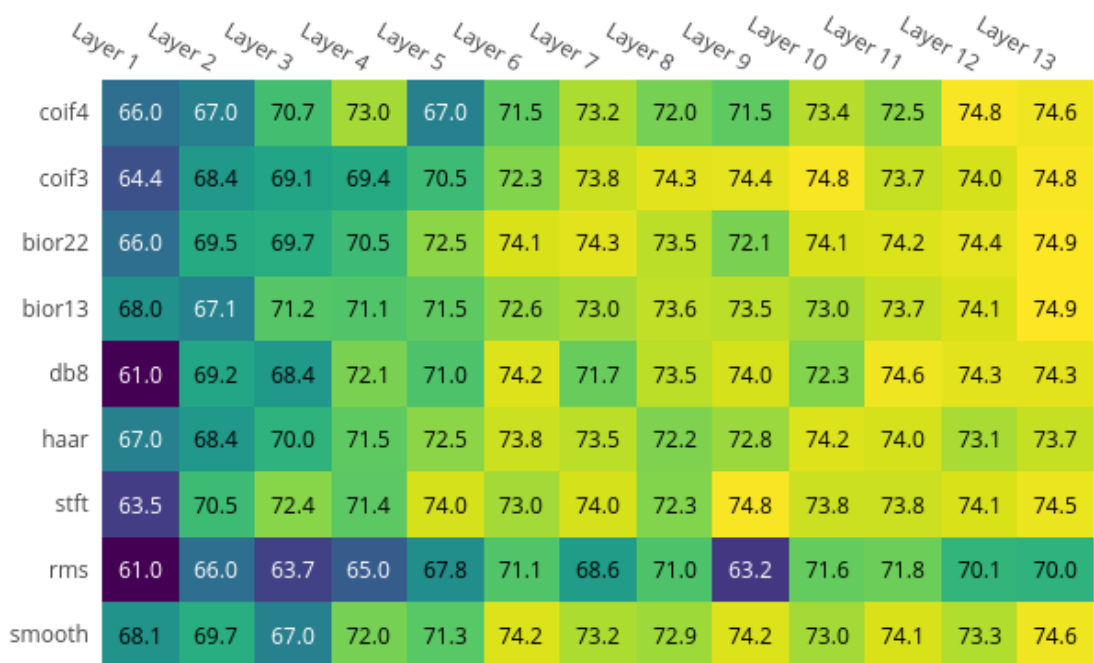
**Table 3.6** Detection accuracies for extension and flexion of finger gestures with calibrated EMGs and trained with a neural network with 8 hidden layers and 5 hidden neurons in each layer.

trained were 42. The duration of the training all of them lasted for 5.2 days. The average time to train every neural net was 2.9 hours.



**Figure 3.3** Average performances of networks from 1 to 13 layers, five neurons each. Each network was trained with the concatenation of sym4sym8 data and tested with 9 other features. The colors represent the names of the features and are shown in the legend box.

---

**Figure 3.4** Heatmap with the detection accuracies



# 4

## Discussion

In this chapter we are going to review the steps of each stage of the pipeline we proposed and we will discuss the presented results of the parameter adjustment phase and the evaluation of the final model.

### 4.1 Parameter Adjustment

Although the testing of the final neural network may not give the optimal detection accuracies, the adjustment of the parameters has proven to increase the detection accuracies. Furthermore, the outputs from the ANNs varies for each initialization so a potential lower or higher detection accuracy may be a result of a random variation. During the process of adjusting the parameter we classified the data between the extension and flexion of the thumb.

#### 4.1.1 Increase on the window step

Firstly, we trained a neural network with one hidden layer and five hidden neurons on each layer. The initial problem we had was that each and every clip of the isolated gestures had different durations. So, we needed to trim them into same duration clips to have a consistent size matrices because MatLab is more efficient with manipulating matrices instead of cells. Thus, on the dataset we extracted for a thumb extension and flexion we applied a window of 128 and a step of 1 between each window and this lead to constructing our same size clips. The result was to extract a lot of data which affected the training time. The training time was 12 days. The detection accuracies for the first experiment proved to be below our expectations. Firstly, to overcome the problem with the training time we decided to increase the step between the different windows. We increased the step from one to 64. When we decreased the amount of the extracted data increasing the windowing step to 64

the accuracies slightly increased as we can see in Fig. 3.2.

### 4.1.2 Forward Selection, Backward Elimination: a hybrid approach

The next combinatorial experiment was conducted to examine which features are performing well when combined in pairs. For the next block of experiments, we decided to combine every two features and then train each pair on a neural network with one hidden layer and 5 hidden neurons and test against the corresponding pair. Table. 3.1 shows us that the best three detection accuracies were between the pair of rms-sym8 with 69.9% accuracy, rms-bior1.3 with 70.0% accuracy and sym4-sym8 with 70.3% accuracy. All the data used in these experiments were extracted using the 64 window step. We can also notice in Table. 3.1 that there is a marginal difference between the detection accuracies of the different duplets. The lowest detection accuracy was noted for the combination of sym8 with bior2.2. However, we cannot exclude the chance of getting these detection accuracies randomly as we know that the outputs of the neural networks are fluctuating on each and every run. Next, we focused on the three best performances and concatenated each pair and used it as a new, fixed pair with which we concatenate each other feature. This resulted in creating a triplet of different features concatenated together and used this triplet to train the neural network. With each different triplet we trained a neural network with one hidden layer and 5 hidden neurons and found the derived detection accuracies. We observe from the Tables. 3.2, 3.3, 3.4 that best detection accuracies are coming from the triplet sym4-sym8. The difference between this triplet and the other two is that the triplet sym4-sym8 is consisted of wavelets with three decomposition levels.

For the next block of experiments we decided to take the best performed triplet which is the sym4-sym8 and combine this triplet with each other feature to train different neural networks. In this block of experiments, we incremented the number of hidden layers by one. Normally, when the detection accuracy stops improving then we stopped increasing the number of hidden layers and focused on the features that performed the best. In our case, since the huge amount of data with the increasing number of hidden layers caused an increasing training time. Thus, we decided to set the maximum limit for 13 layers. In the Table. 3.5 we see that for the triplet sym4-sym8-rms the detection accuracy follows an arbitrary pattern and noted the lowest performance as well. We note here that the features with the best constantly increasing performance are the wavelets and in particular bior2.2 and coif3. In the following Fig. 3.4 we can see the fluctuating values between the different features for each number of layers which we used in the neural networks.

## 4.2 Evaluation results

According to the results we received from the classification of the evaluation data in Table. 3.6 we can not receive a confident picture of which of the features are

performing well. We observe that our neural model underperformed for some gestures and performed better for some other gestures. For example, we noted the best performance for all the three features for the extension and flexion of the pinky finger. For the detection accuracy of the finger gesture G9 which is the data we acquired from the extension and flexion of the thumbs from the 21 subjects we can conclude that there is not an overfitting. Below we will show some statistics from the performance of our neural network with the new acquired data based on the results from the Table 3.6.

The average performance per feature is depicted below:

sym4sym8			
Features	db8	bior2.2	coif3
Average performance	63.4%	66.15%	63.0%

**Table 4.1** Average detection accuracies per feature from Table 3.6

The average detection accuracy between the different finger gestures is depicted below:

sym4sym8			
Gestures	Average performance	Gestures	Average performance
G1	63.0%	G8	66.9%
G2	68.6%	G9	63.3%
G3	67.3%	G10	67.1%
G4	61.7%	G11	70.4%
G5	53.8%	G12	59.7%
G6	73.9%	G13	68.1%
G7	54.5%	G14	59.5%

**Table 4.2** Average detection accuracies per finger gesture from Table 3.6

The variance in the results can be justified because the acquired signals are coming from 21 different subjects where the majority of them executed the protocolled finger gestures slightly differently. What's more, the height of the placement of the Myo armband on the forearm could not be in all 21 subjects exactly same but it was estimated approximately. That means that the acquired signals might be recorded from different forearm muscles from subject to subject. Furthermore, the signals from different fingers have varying amplitude which could lead to a biased performance of the classification algorithm. Also, the fact that multiple muscles are flexing and extending the fingers can affect the results of the classification algorithm. We observed also, that the majority of the subjects when flexing and extending their pinky finger caused the ring finger to get strained as well. Last but not least the EMG's amplitude and frequency is affected by each subject's percent of fat, muscle tissue, hairiness, muscular fatigue, the subject's age, neuromuscular diseases and the temperature of the skin.

A lot of literature related to our work can be found yet there are some basic differences in the tools that were used. In the work of Vijayan et al. [55], they acquired 6-channel EMG signals from the flexion of the five fingers of the hand and for the classification they used Multi class SVMs. Their classification results for the flexions of the thumb, index, middle, ring and pinky were 100%, 88.8%, 94.4%, 100%, 83.3% respectively.

In the work of Abreu et al. [56] they acquired EMG signals with the Myo armband regarding the recognition of gestures of the LIBRAS (Brazilian Sign Language) alphabet. For the classification of the 20 different hand gestures they used SVMs. In their real time evaluation they had good performances for the letters that could be easily performed with strength and as for the gestures that could not be performed with strength or because their gestures are similar to the gestures of other letters the classifier's performance proofed to be worse.

In the work of Benalcázar et al. [57] they developed an online system that could classify with 86% detection accuracy on the contrary with 83% detection accuracy of the Myo proprietary software on five different hand gestures such as pinch, fist, open, wave in and wave out. For the feature extraction they used rectification of the signal combined with a low-pass Butterworth filter because it reduces the noises and smooths each channel and they classified the different hand gestures with the k-NN classification algorithm.

In the work of Côté-Allard et al. [58] they recorded two datasets from the forearms of 19 and 17 able-bodied participants and they used the first dataset for the pre-training and the second dataset for the evaluation. They proposed two separate convolutional deep neural networks one for the CWT data and one for the STFT data. They concluded that the CWT-convolutional neural network outperformed the STFT-based with an average accuracy of 98.31% for the recognition of 7 hand gestures in 17 participants.

In the work of Atzori et al. [59] they proposed a Convolutional Neural Network for the classification of 50 hand movements acquired from 67 intact subjects and 11 transradial amputees. The whole dataset was divided into 3 subsets. The average classification accuracy of the convolutional neural network was 66.5% on the first dataset which and 60.27% for the second dataset. For the third dataset which consisted only from the signal of the amputees, the convolutional neural network had an accuracy of 38.09%. To acquire the signals from the amputees they were asked to imagine imitating the movements with the missing hand as naturally as possible.

# 5

## Conclusion

In this thesis a classification pipeline has been developed to detect 14 different finger gestures using solely EMG signals. This chapter provides a summary of this thesis and explains the reasons behind the choices that were made. Future suggestions to improve the existed EMG method are also included in the section 5.1.

To build an ideal EMG based gesture recognition system should consist of an EMG signal analysis system which is precise, quick and credible. However, the purpose of this thesis is not to develop a complete functional system but rather to explore the performance of a feed forward neural network when its input is consisting of different extracted features from the EMG signals.

In this work, we proposed an EMG method for the classification of finger gestures from intact subjects. For the classification we decided to experiment with a feed-forward neural network. In order to adjust correctly the parameters for our neural network we used as initial input EMG signals from my forearm for the flexion and the extension of the thumb with the palm facing upwards.

The motive of this work is to examine a majority of possibilities of using machine learning to classify EMG data. This work only supports the simplest neural network architecture, the fully connected feed forward neural networks. In this work we experiment with one kind of network architecture the Multi-layer Perceptron with the focus to determine which parameters are of great significance to the accuracy and possibly performance.

We decided to follow a hybrid approach of the forward selection, backward elimination. We started training a neural network of one hidden layer and 5 hidden neurons with all the possible duplets of the existing features. After the training, we tested also the trained neural networks and we got the detection accuracies. From the detection accuracies we got the 3 best performances. We combined each of the best three duplets with the rest features and trained another neural network with one hidden layer and five hidden neurons. The duplet with the best detection performance was chosen and we used that duplet to combine with the rest features forming triplets. With each triplet we trained feed-forward neural networks with one hidden layer and five hidden neurons but this time incrementing the number of

hidden layers by one.

The limitation of time did not allow us to experiment with other parameters than the number of hidden layers. The maximum number of hidden layers we reached was 13. For decided for the evaluation of the data we would a number of hidden layers which would not be close to the maximum number of layers in order to avoid possible overfitting of the evaluation data. We decided to choose 8 hidden layers for the final neural network. For that decision the Fig. 3.3 helped us to come to the conclusion that the beginning of the plateau of the accuracies started to form around for 8 hidden layers. For that specific number of hidden layers we noted which triplets gave the best detection accuracies.

For the evaluation stage we created a database consisting solely of EMG signals coming from 14 finger gestures of 21 intact subjects. Each finger gesture is consisting of one flexion and one extension. As aforementioned, the final neural network had 8 hidden layers with 5 hidden neurons each. Furthermore, the final training did not happen with all the possible triplets but only for the best performed during the process of the parameter adjustment. For each finger gesture a classifier was built in order to distinguish between the extension and the flexion and the final corresponding detection accuracy was noted.

Based on the results we received, we believe it is difficult to distinguish delicate finger gestures only with EMG data and that classifiers would perform poorly if we are to compare them with other vision techniques or wearable gloves. Although, the importance of the results they make us believe that EMG data could be used as an addition to systems that also depend on other types of data. One of the most significant characteristics of the Myo armband is that its EMG sensors are portable. Regarding the fact that the basis for a successful gesture recognition system are portability and convenience we believe that a hybrid approach using both visual and EMG data could be robust, compact and considerably less cumbersome than wearable gloves.

## 5.1 Future Work

In this section we will provide potential improvements to the current pipeline.

### 5.1.1 Size of data

Creating a huge dataset to include all the relevant variations helps us to resolve to a great extent the problem of considerable changes in EMG signals from person to person, as we already mentioned. This will also improve the robustness of the EMG signals regardless the potential changes of the Myo's position on the subject's arm.

### 5.1.2 Amount of features and reduction of the feature vector

For this work, we used only 11 features to extract useful information. We recommend for the further exploration of the EMG signals the use of more features on them that performed well on other works similar to ours but did not apply them on this work. For example, for the further adjustment of the preprocessing phase we recommend:

- to experiment with the window size for the windowing part.
- test more discrete wavelets and different decompositiong levels.
- further experiment with the continuous wavelet transform as an alternative to DWT.

What's more, the size of the final feature vector which we used was big enough and this leads to a long run time. For the future exploration of the existing finger gesture database we recommend the application of a method which has as purpose the reduction of the dimension of the final feature vector such as the Principal Component Analysis (PCA) or Linear Discriminant Analysis (LDA).

### 5.1.3 Network Architectures

This work is based on a simple feed forward network architecture. We encourage the further experimentation with other kinds of network architectures. In case we keep the time information along with the amplitude of the EMG signal we can use the Recurrent Neural Network architecture (RNN) which has the ability to remember and make use of the sequential information. This feature can be useful for analyzing a sequence of gestures.

Another deep learning architecture which is recently widely used achieving a considerable performance is the Convolutional Neural Network (CNN) architecture [60, 61]. Even though CNN architecture is used in image analysis, it has also its applications on time-series data, such as speech recognition [62] and gesture recognition [59] .



# Bibliography

- [1] Myo;. Available from: <https://myo.com>.
- [2] Ziegler-Graham K, MacKenzie EJ, Ephraim PL, Travison TG, Brookmeyer R. Estimating the prevalence of limb loss in the United States: 2005 to 2050. Archives of physical medicine and rehabilitation. 2008;89(3):422–429.
- [3] Owings MF, Kozak LJ. Ambulatory and inpatient procedures in the United States, 1996. Vital and health statistics Series 13, Data from the National Health Survey. 1998;(139):1–119.
- [4] Varma P, Stineman MG, Dillingham TR. Physical Medicine and Rehabilitation Clinics of North America Epidemiology of Limb Loss. Physical medicine and rehabilitation clinics of North America. 2014 Feb;25(1):1–8. Available from: <https://www.ncbi.nlm.nih.gov/pmc/articles/PMC4533906/>.
- [5] Robbins JM, Strauss G, Aron D, Long J, Kuba J, Kaplan Y. Mortality rates and diabetic foot ulcers: is it time to communicate mortality risk to patients with diabetic foot ulceration? Journal of the American Podiatric Medical Association. 2008;98(6):489–493.
- [6] Tenore F, Ramos A, Fahmy A, Acharya S, Etienne-Cummings R, Thakor NV. Towards the control of individual fingers of a prosthetic hand using surface EMG signals. In: Engineering in Medicine and Biology Society, 2007. EMBS 2007. 29th Annual International Conference of the IEEE. IEEE; 2007. p. 6145–6148.
- [7] Dillingham TR, Pezzin LE, MacKenzie EJ. Limb amputation and limb deficiency: epidemiology and recent trends in the United States. Southern medical journal. 2002;95(8):875–884.
- [8] Weir RF, Grahn EC. Persons with partial hand amputations. In: Engineering in Medicine and Biology Society, 2000. Proceedings of the 22nd Annual International Conference of the IEEE. vol. 1. IEEE; 2000. p. 427–430.
- [9] Zhang Y, Harrison C. Tomo: Wearable, low-cost electrical impedance tomography for hand gesture recognition. In: Proceedings of the 28th Annual ACM Symposium on User Interface Software & Technology. ACM; 2015. p. 167–173. Available from: <http://dl.acm.org/citation.cfm?id=2807480>.
- [10] Shin S, Sung W. Dynamic hand gesture recognition for wearable devices with low complexity recurrent neural networks. In: 2016 IEEE International Symposium on Circuits and Systems (ISCAS); 2016. p. 2274–2277.

- [11] Kakoty NM, Saikia A, Hazarika SM. Exploring a family of wavelet transforms for EMG-based grasp recognition. *Signal, Image and Video Processing*. 2015;9(3):553–559. Available from: <http://link.springer.com/article/10.1007/s11760-013-0477-7>.
- [12] Zhao Z, Chen X, Zhang X, Yang J, Tu Y, Lantz V, et al. Study on online gesture sEMG recognition. *Advanced Intelligent Computing Theories and Applications With Aspects of Theoretical and Methodological Issues*. 2007;p. 1257–1265. Available from: <http://www.springerlink.com/index/G771691106786P23.pdf>.
- [13] Nod;. Available from: <https://nod.com>.
- [14] Mycestro;. Available from: <http://www.mycestro.com/>.
- [15] Nymoen K, Haugen MR, Jensenius AR. Mumyo—evaluating and exploring the myo armband for musical interaction; 2015. Available from: <https://www.duo.uio.no/handle/10852/43980>.
- [16] Meet the Man With a Myo-Controlled Robotic Arm;. Available from: <http://developerblog.myo.com/meet-the-man-with-a-myo-controlled-robotic-arm/>.
- [17] Kutafina E, Laukamp D, Jonas SM. Wearable Sensors in Medical Education: Supporting Hand Hygiene Training with a Forearm EMG. Västeras, Sweden; 2015. Available from: <http://ebooks-iospress.nl/publication/39272>.
- [18] Yang C, Chang S, Liang P, Li Z, Su CY. Teleoperated robot writing using emg signals. In: *Information and Automation, 2015 IEEE International Conference on*. IEEE; 2015. p. 2264–2269.
- [19] Dash A, Sahu A, Shringi R, Gamboa JCB, Afzal MZ, Malik MI, et al. AirScript-Creating Documents in Air. *arXiv preprint arXiv:170511181*. 2017;
- [20] Kosmidou VE, Hadjileontiadis LJ. Sign language recognition using intrinsic-mode sample entropy on sEMG and accelerometer data. *IEEE transactions on biomedical engineering*. 2009;56(12):2879–2890. Available from: <http://ieeexplore.ieee.org/abstract/document/4760276/>.
- [21] Cheng B, Liu G. Emotion recognition from surface EMG signal using wavelet transform and neural network. In: *Proceedings of The 2nd International Conference on Bioinformatics and Biomedical Engineering (ICBBE)*; 2008. p. 1363–1366. Available from: [http://www.paper.edu.cn/en\\_releasepaper/downPaper/200706-289](http://www.paper.edu.cn/en_releasepaper/downPaper/200706-289).
- [22] Ververidis D, Karavarsamis S, Nikolopoulos S, Kompatsiaris I. Pottery gestures style comparison by exploiting Myo sensor and forearm anatomy. In: *Proceedings of the 3rd International Symposium on Movement and Computing*. ACM; 2016. p. 3. Available from: <http://dl.acm.org/citation.cfm?id=2948924>.
- [23] Portable EMG/EP system;. Available from: [https://www.alibaba.com/product-detail/Portable-EMG-EP-system\\_1489243551.html?spm=a2700.7724857.main07.27.144bb7b6J31hPy](https://www.alibaba.com/product-detail/Portable-EMG-EP-system_1489243551.html?spm=a2700.7724857.main07.27.144bb7b6J31hPy).

- [24] Disposable Hypodermic Needle Electrodes;. Available from: <https://digitimer.com/products/clinical-neurophysiology/neurodiagnostic-accessories/disposable-hypodermic-needle-electrodes/>.
- [25] EMG surface electrodes;. Available from: <http://medimaxtech.com/trio-electrodes/>.
- [26] Winter DA, Fuglevand AJ, Archer SE. Crosstalk in surface electromyography: theoretical and practical estimates. *Journal of Electromyography and Kinesiology*. 1994;4(1):15–26.
- [27] Non-stationary nature of speech signal (theory);. Available from: <http://iitg.vlab.co.in/?sub=59&brch=164&sim=371&cnt=1104>.
- [28] Bonato P, Roy SH, Knaflitz M, De Luca CJ. Time-frequency parameters of the surface myoelectric signal for assessing muscle fatigue during cyclic dynamic contractions. *IEEE Transactions on Biomedical Engineering*. 2001;48(7):745–753.
- [29] Thalmic blog;. Available from: <http://blog.thalmic.com/>.
- [30] Myo Developer;. Available from: <https://developer.thalmic.com/>.
- [31] Logging IMU and Raw EMG Data;. Available from: <http://developerblog.myo.com/myocraft-logging-imu-and-raw-emg-data/>.
- [32] Raw and Uncut Drops Today;. Available from: <http://developerblog.myo.com/raw-uncut-drops-today/>.
- [33] Dietterich T. Machine learning for sequential data: A review. *Structural, syntactic, and statistical pattern recognition*. 2002;p. 227–246.
- [34] Whittaker ET, Robinson G. *The calculus of observations: An introduction to numerical analysis*. Dover Publications; 1924.
- [35] Kenney JF. *Mathematics of statistics*. D. Van Nostrand Company Inc; Toronto; Princeton; New Jersey; London; New York,; Affiliated East-West Press Pvt-Ltd; New Delhi; 2013.
- [36] Sethares WA. *Rhythm and transforms*. Springer Science & Business Media; 2007.
- [37] Polikar R. The wavelet tutorial. 1996;Available from: [http://person.hst.aau.dk/enk/ST8/wavelet\\_tutorial.pdf](http://person.hst.aau.dk/enk/ST8/wavelet_tutorial.pdf).
- [38] Lee DT, Yamamoto A. Wavelet analysis: theory and applications. *Hewlett Packard journal*. 1994;45:44–44.
- [39] Wavelet Toolbox Overview;. Available from: <https://de.mathworks.com/videos/wavelet-toolbox-overview-115893.html>.
- [40] Giurgiutiu V, Yu L. Comparison of short-time fourier transform and wavelet transform of transient and tone burst wave propagation signals for structural health monitoring. In: Proceedings of 4th international workshop on structural health monitoring; 2003. p. 1267–1274.

- [41] Mao KZ. Orthogonal forward selection and backward elimination algorithms for feature subset selection. *IEEE Transactions on Systems, Man, and Cybernetics, Part B (Cybernetics)*. 2004;34(1):629–634.
- [42] Jović A, Brkić K, Bogunović N. A review of feature selection methods with applications. In: *Information and Communication Technology, Electronics and Microelectronics (MIPRO), 2015 38th International Convention on*. IEEE; 2015. p. 1200–1205.
- [43] Goodfellow I, Bengio Y, Courville A. *Deep Learning*. MIT Press; 2016. <http://www.deeplearningbook.org>.
- [44] NEUROBIOLOGY NEURODEVELOPMENT: NATURE AND NUTURE;. Available from: <http://www.4mylearn.org/Neurobiology.html>.
- [45] Hinton G, Deng L, Yu D, Dahl GE, Mohamed Ar, Jaitly N, et al. Deep neural networks for acoustic modeling in speech recognition: The shared views of four research groups. *IEEE Signal Processing Magazine*. 2012;29(6):82–97.
- [46] Girshick R, Donahue J, Darrell T, Malik J. Rich feature hierarchies for accurate object detection and semantic segmentation. In: *Proceedings of the IEEE conference on computer vision and pattern recognition*; 2014. p. 580–587.
- [47] Gawehn E, Hiss JA, Schneider G. Deep learning in drug discovery. *Molecular informatics*. 2016;35(1):3–14.
- [48] Park Y, Kellis M. Deep learning for regulatory genomics. *Nature biotechnology*. 2015;33(8):825–826.
- [49] Dechter R. Learning while searching in constraint-satisfaction problems. University of California, Computer Science Department, Cognitive Systems Laboratory; 1986.
- [50] Deng L. Three classes of deep learning architectures and their applications: a tutorial survey. *APSIPA transactions on signal and information processing*. 2012;.
- [51] Mikolov T, Karafiat M, Burget L, Černocky J, Khudanpur S. Recurrent neural network based language model. In: *Eleventh Annual Conference of the International Speech Communication Association*; 2010. .
- [52] Gelfand IM, Silverman RA. *Calculus of variations*. Courier Corporation; 2000.
- [53] McCormick C. Gradient Descent Derivation; 2014. Available from: <http://mccormickml.com/2014/03/04/gradient-descent-derivation/>.
- [54] Kapur R. Neural Networks and The Backpropagation Algorithm, Explained; 2016. Available from: <https://ayearofai.com/rohan-lenny-1-neural-networks-the-backpropagation-algorithm-explained-abf4609d4f9d>.
- [55] Vijayan AE, John A, Sudheer AP. Surface electromyography based finger flexion recognition. In: *Computational Intelligence & Communication Technology (CICT), 2015 IEEE International Conference on*. IEEE; 2015. p. 592–596. Available from: <http://ieeexplore.ieee.org/abstract/document/7078772/>.

- [56] Abreu JG, Teixeira JM, Figueiredo LS, Teichrieb V. Evaluating sign language recognition using the myo armband. In: Virtual and Augmented Reality (SVR), 2016 XVIII Symposium on. IEEE; 2016. p. 64–70.
- [57] Benalcázar ME, Jaramillo AG, Zea A, Páez A, Andaluz VH. Hand gesture recognition using machine learning and the Myo armband. In: Signal Processing Conference (EUSIPCO), 2017 25th European. IEEE; 2017. p. 1040–1044.
- [58] Côté-Allard U, Fall CL, Drouin A, Campeau-Lecours A, Gosselin C, Glette K, et al. Deep Learning for Electromyographic Hand Gesture Signal Classification by Leveraging Transfer Learning. arXiv preprint arXiv:180107756. 2018;.
- [59] Atzori M, Cognolato M, Müller H. Deep learning with convolutional neural networks applied to electromyography data: a resource for the classification of movements for prosthetic hands. Frontiers in neurorobotics. 2016;10:9.
- [60] Schmidhuber J. Deep learning in neural networks: An overview. Neural networks. 2015;61:85–117.
- [61] He K, Zhang X, Ren S, Sun J. Deep residual learning for image recognition. In: Proceedings of the IEEE conference on computer vision and pattern recognition; 2016. p. 770–778.
- [62] Qian Y, Woodland PC. Very deep convolutional neural networks for robust speech recognition. In: Spoken Language Technology Workshop (SLT), 2016 IEEE. IEEE; 2016. p. 481–488.



# List of Figures

1.1	Disposable Hypodermic Needle Electrodes[24]	4
1.2	EMG Surface Electrodes[25]	5
1.3	Sine wave of 10 Hz sampled using a sampling frequency of 1000 Hz.	6
1.4	Multitone sine wave of 10, 50 and 100 Hz sampled using a sampling frequency of 1000 Hz.	6
1.5	Non-stationary multitone sine wave of 10, 50 and 100 Hz sampled using a sampling frequency of 1000 Hz.	7
1.6	Myo armband	9
1.7	Gestures recognized by Myo	9
1.8	EMG channel assignments	10
1.9	Positioning of Myo in user's forearm. [32]	11
2.1	Overview of the pipeline	14
2.2	Data collection	14
2.3	Division of recording into 5 folds	15
2.4	Windowing	17
2.5	Application of the STFT in the segmented windows [36]	18
2.6	Spectrograms of the thumb extension	19
2.7	Spectrogram of the thumb extension from Myo's 7th channel	21
2.8	Spectrogram of the thumb flexion from Myo's 7th channel	21
2.9	Wavelet families [39]	22
2.10	The subband coding algorithm	24
2.11	Feature extraction	26
2.12	Training & classification: For the training part we concatenate the n-th training fold with the extension and the flexion data for each of the extracted features. We proceed by training the model with these data. Then, we concatenate the n-th test fold for the extension and flexion data and for the same feature as we did for the training folds. After testing the newly trained neural network with the test data we have the detection accuracies.	27

2.13 Anatomy of a biological neuron [44] . . . . .	29
2.14 Artificial neuron . . . . .	30
2.15 Feed-forward network . . . . .	31
2.16 Common activation functions used in artificial neural networks along with their derivatives. . . . .	35
2.17 Convex function $z = x^2 + y^2$ . . . . .	39
2.18 Convex function $y = x^2$ . . . . .	40
2.19 Double layered neural network . . . . .	41
2.21 14 finger gestures from 21 different subjects were acquired using the Myo armband . . . . .	45
3.1 Average performances with one hidden layer, five neurons and step one	48
3.2 Average performances with one hidden layer, five neurons and step 64	49
3.3 Average performances of networks from 1 to 13 layers, five neurons each. Each network was trained with the concatenation of sym4sym8 data and tested with 9 other features. The colors represent the names of the features and are shown in the legend box. . . . .	52
3.4 Heatmap with the detection accuracies . . . . .	53

# List of Tables

2.1	The values of W prior to each iteration and the update amounts . . . . .	40
3.1	Combined features and ran on neural net with one hidden layer and five hidden neurons. . . . .	50
3.2	Combined features per 3 and ran on neural net with one hidden layer and five hidden neurons. . . . .	50
3.3	Combined features per 3 and ran on neural net with one hidden layer and five hidden neurons. . . . .	50
3.4	Combined features per 3 and ran on neural net with one hidden layer and five hidden neurons. . . . .	50
3.5	Best three performances per layer. Combined features per 3 and ran on neural net with incrementing the number of layers from one to eight. . . . .	51
3.6	Detection accuracies for extension and flexion of finger gestures with calibrated EMGs and trained with a neural network with 8 hidden layers and 5 hidden neurons in each layer. . . . .	51
4.1	Average detection accuracies per feature from Table 3.6 . . . . .	57
4.2	Average detection accuracies per finger gesture from Table 3.6 . . . . .	57



# A

## Appendix

### A.1 List of Abbreviations

EMG	Electromyography
ANN	Artificial Neural Network
CWT	Continuous Wavelet Transform
DWT	Discrete Wavelet Transform
IMU	Inertia Measurement Unit
AI	Artificial Intelligence
MLP	Multilayer Perceptron
MSE	Mean Squared Error